Paternal transmission of the Wolbachia CidB toxin underlies cytoplasmic incompatibility

Béatrice Horard, Kevin Terretaz, Anne-Sophie Gosselin-Grenet, Hélène Sobry, Mathieu Sicard, Frederic Landmann, Benjamin Loppin

Paternal transmission of the *Wolbachia* CidB toxin underlies Cytoplasmic Incompatibility

Béatrice Horard[1], Kevin Terretaz[2], Anne-Sophie Gosselin-Grenet[3], Hélène Sobry[3], Mathieu Sicard[4], Frédéric Landmann[2]*, Benjamin Loppin[1]*

[1] LBMC, École Normale Supérieure de Lyon, CNRS UMR5239, Université de Lyon, 46 allée d'Italie, 69007 Lyon, France.

[2] CRBM, Université de Montpellier, CNRS, 1919 Route de Mende, 34293 Montpellier, France.

[3] DGIMI, Université de Montpellier, INRAE, Place Eugène Bataillon, 34295 Montpellier, France.

[4] ISEM, Université de Montpellier, CNRS, IRD, Place Eugène Bataillon, 34295 Montpellier, France.

*Correspondence: frederic.landmann@crbm.cnrs.fr and benjamin.loppin@ens-lyon.fr

Lead contact: Benjamin Loppin (benjamin.loppin@ens-lyon.fr)

Keywords:

Wolbachia, Cytoplasmic Incompatibility, *Drosophila*, *Culex*, Toxin-Antidote, spermiogenesis, fertilization, DNA replication stress, CidA, CidB

Summary

Wolbachia are widespread endosymbiotic bacteria that manipulate the reproduction of arthropods through a diversity of cellular mechanisms. In Cytoplasmic Incompatibility (CI), a sterility syndrome originally discovered in the mosquito *Culex pipiens*, uninfected eggs fertilized by sperm from infected males are selectively killed during embryo development following the abortive segregation of paternal chromosomes in the zygote. Despite the recent discovery of *Wolbachia* CI factor (*cif*) genes, the mechanism by which they control the fate of paternal chromosomes at fertilization remains unknown. Here, we have analyzed the cytological distribution and cellular impact of CidA and CidB, a pair of Cif proteins from the *Culex*-infecting *Wolbachia* strain *w*Pip. We show that expression of CidB in *Drosophila* S2R+ cells induces apoptosis unless CidA is co-expressed and associated with its partner. In transgenic *Drosophila* testes, both effectors colocalize in germ cells until the histone-to-protamine transition where only CidB is retained in maturing spermatid nuclei. We further show that CidB is similarly targeted to maturing sperm of naturally-infected *Culex* mosquitoes. At fertilization, CidB associates with paternal DNA regions exhibiting DNA replication stress, as a likely cause of incomplete replication of paternal chromosomes at the onset of the first mitosis. Importantly, we demonstrate that inactivation of the deubiquitylase activity of CidB does not abolish its cell toxicity or its ability to induce CI in *Drosophila*. Our study thus demonstrates that CI functions as a transgenerational Toxin-Antidote system, and suggests that CidB acts by poisoning paternal DNA replication in incompatible crosses.

Introduction

Wolbachia are intracellular bacteria of the order Rickettsiales that infect several classes of arthropods as well as filarial nematodes[1,2]. First described in the gonads of the mosquito *Culex pipiens* as symbiotic Rickettsia-like bacteria[3], *Wolbachia* are widespread in most insect orders. These endosymbionts are well known for their ability to manipulate the reproduction of their hosts through an impressive diversity of sophisticated mechanisms that all favor their vertical transmission through the female germline[1,2].

Cytoplasmic Incompatibility (CI), a sterility syndrome also discovered in *Culex*[4], is the most prevalent reproductive parasitic mechanism deployed by *Wolbachia*[5]. By allowing the selective development of infected eggs when fertilization involves a sperm from an infected male, CI efficiently contributes to the strict matriline spreading of *Wolbachia* in insect populations[6]. Combined with the ability of *Wolbachia* to suppress viral infection, the local release of infected *Aedes aegypti* mosquitoes is successfully used to control the transmission of pathogenic arboviruses to human populations[7].

Incompatible crosses between an infected male and an uninfected female, or between parents harboring mutually incompatible *Wolbachia* strains, lead to defective segregation of paternal chromosomes at the first embryonic division, a phenotype that causes embryonic death in diploid species[8,9]. The first manifestation of this phenotype is a delayed or abnormal progression of paternal chromosomes into the first nuclear cycle, leading to replication defects and abnormal compaction of paternal chromosomes in metaphase[10,11]. As maternal chromosomes present within the same mitotic spindle enter anaphase, paternal chromosomes are either left behind or form a chromatin bridge between the two daughter nuclei. Depending on the severity of these early defects, paternal chromosomes can be lost at the first mitosis or can persist for a few additional divisions, leading to the formation of haploid or aneuploid embryos, respectively[12]. These defects are

generally lethal for embryos, but the strength of CI, as measured by embryo hatching rate, vary considerably from one species to another. For instance, in *D. melanogaster*, CI is typically very low in standard crossing schemes, whereas it is strong in *Drosophila simulans* and fully lethal in most incompatible crosses of *Culex pipiens*[13,14]. An intriguing aspect of CI is the remarkable conservation of these cytological phenotypes across insect orders harboring distant *Wolbachia* strains[12-15]. Furthermore, *Wolbachia* are capable of inducing CI when transferred into a new host, suggesting that CI affects highly conserved host targets or cellular processes[13,16,17].

A diversity of potential molecular mechanisms contributing to CI have been reported in the past fifteen years[18-22]. In addition, several theoretical models of CI have emerged from decades of active research[23-28]. For instance, the early *mod-resc* model proposed a two loci system consisting of a bacterial, sperm modifier (*mod*) factor expressed in testes and a rescue (*resc*) factor present in eggs[24]. As a variation on this theme, the "lock and key" model later proposed a direct interaction of the two predicted *Wolbachia* gene products at fertilization[25]. In its latest form, this model of CI, named Toxin-Antidote (TA)[26], integrates the recent discovery of CI factor (*cifs*) genes, collectively known as *cifA* and *cifB*[29,30]. *cifs* genes are expressed as one or several operons present within the WO prophage genomic region and are only found in CI-inducing *Wolbachia* strains[31]. Functional analysis of *cifA* and *cifB* expressed as transgenes in *Drosophila melanogaster* have revealed that while *cifB* is required to induce CI, *cifA* is essential for the rescue of compatible eggs [26,29,30,32,33]. The remarkable ability of CifA to bind CifB *in vitro* and to neutralize a temperature-dependent toxic effect of CifB on the growth of yeast cells have suggested the possibility that these proteins function as a TA system[29]. The TA model posits that spermatozoa from infected males transport the CifB toxin to the egg, which causes abnormal condensation and segregation of paternal

chromosomes during the first zygotic nuclear cycle[28]. These chromosomal defects can be prevented or "rescued" by the presence of the CifA antidote in eggs from infected females. In an alternative model named Host-Modification (HM), Cifs proteins modify sperm chromatin in a way that impedes paternal chromosome division in the egg unless these modifications are reversed by maternally provided CifA[5]. In contrast to the TA model, the HM model does not imply that the effectors reside in the male gamete. Therefore, establishing the distribution and cellular impact of Cifs *in vivo* could prove crucial in distinguishing between these opposing models. Here, we have examined the distribution and function of a pair of Cifs proteins from a *w*Pip *Wolbachia* strain infecting *Culex* mosquitoes, in three independent biological systems. Our cytological and functional analyses are in full support of the TA model of CI and bring new insights about the impact of CidB on paternal chromosomes at fertilization.

Results

Expression of CidA and CidB effectors in *Drosophila* S2R+ cells recapitulates a toxin-antidote system

To conduct our cytological analyses of Cifs proteins, we chose to focus on *Wolbachia* Type I CI effectors $CidA^{wPip}$ and $CidB^{wPip}$ (hereafter CidA and CidB, but also known as $CifA_{wPip[T1]}$ and $CifB_{wPip[T1]}$ in a concurrent nomenclature[33]), one of the most extensively characterized pair of effectors, so far[29,34,35]. Most *w*Pip *Wolbachia* strains characterized in *Culex pipiens* mosquitoes induce full CI when males are crossed with uninfected females[4,5] and dual transgenic expression of CidA and CidB in *Drosophila* also induce a full CI-like phenotype in this model species[29]. The CidB toxin harbors four non-canonical and inactive PD-(D/E)XK nuclease domains as well as a C-terminal DUB (also named Ubiquitin-like protease 1 – Ulp1) domain, which is also present in Type 1 CifB

from *w*Mel, a *Wolbachia* strain infecting *D. melanogaster*. Recent structural analyses have shown that CifA and CifB form stable heterodimers *in vitro* with their cognate partner[34].

To get insights into the distribution and impact of these effectors in insect cells, fluorescent protein fusions of CidA (mKate2::CidA) and CidB (sfGFP::CidB) were expressed in *Drosophila* S2R+ cells either separately or as dual expression constructs (**Figure 1A**). When cells are transfected with the dual construct, both fCidA and fCidB remain strictly cytoplasmic in interphase but accumulate on chromatin during mitosis. Surprisingly, when individually-expressed, fCidA retains this dynamic distribution but fCidB localizes in the nucleus in interphase (**Figure 1A**). This dramatic change in distribution of fCidB between dual and single expression strongly suggests that both effectors interact *in cellulo* as they do *in vitro*[29,34] and that fCidA is capable of sequestrating its partner in the cytoplasm. Remarkably, we noticed that fCidB expression alone induced 100% cell death before division (**Figure 1A,B** and **Video S1)**, an effect which is reminiscent of its negative impact on the growth of yeast cells in heterologous expression experiments[29,36]. Finally, co-expression of fCidA and fCidB restored growth rate similar to control transfection with the empty vector (**Figure 1B** and **Video S2**). The behavior of fCidA and fCidB in *Drosophila* S2R+ cells is thus similar to a bacterial type II toxin-antitoxin system, where the CidA antitoxin (or antidote) is capable of neutralizing the CidB toxin through a direct interaction[37,38].

The cellular toxicity of CidB is independent of its deubiquitylase activity

The DUB domains of Type I CifBs from *w*Mel and *w*Pip *Wolbachia* have been functionally implicated in the induction of a CI-like phenotype in transgenic *D. melanogaster*[29,32]. Specifically, replacing the catalytic cysteine residue of the DUB with an alanine (C>A) blocks its activity *in vitro* and restores fertility to transgenic males. Importantly, this single amino-acid change strongly reduces CidB toxicity when expressed

in yeast cells at the restrictive temperature[29]. However, to our surprise, expression of this same catalytic mutant (fCidB^{C1025A}) in S2R+ cells was still highly toxic and induced apoptosis in a way indistinguishable to wild-type fCidB (**Figure 1A,B**). Western-Blot analyses revealed similar expression levels of wild-type and mutant fCidB, thus ruling out a dosage effect (**Figure S1**). Although the C>A replacement efficiently blocks DUB activity, it does not prevent substrate recognition and can even increase the affinity of the mutated DUB for ubiquitin, with unpredictable effects. In contrast, a C>R substitution blocks DUB activity but also decreases the affinity for ubiquitin in tested DUB proteins[39]. We thus analyzed the effect of this mutation on the fCidB transgene (fCidB^{C1025R}). Our results clearly show that CidB^{C1025R} is still highly toxic in S2R+ cells (**Figure 1A,B**), thus confirming that CidB kills S2R+ cells in a DUB-independent manner.

The CidB toxin is loaded in spermatid nuclei at the histone-to-protamine transition

To extend these observations *in vivo*, we used a *Drosophila* transgenic line[29] expressing tagged versions of this same pair of *w*Pip effectors under the control of the UAS/Gal4 system (*UAS-V5::CidA-T2A-FLAG::CidB*, hereafter *UAS-tCidA-tCidB*) (**Figure 2A**). The T2A self-cleaving peptide allows the production of both effectors from a single ORF, thereby mimicking the activity of a bacterial operon[40]. As a pilot experiment, we first activated the transgene in larval salivary glands, which contain the giant polytene chromosomes, using the *Sgs3-Gal4* driver[41]. Immunofluorescence against the protein tags (V5 and FLAG, respectively) revealed a perfect co-localization of tCidA and tCidB on polytene chromosome bands, thus confirming their mutual association and their general affinity with chromatin (**Figure 2B**). Interestingly, within the same salivary glands, we also observed cells where the effectors were present in the cytoplasm, where they again colocalized (**Figure 2B**).

To study the distribution of these *Wolbachia* effectors in *Drosophila* testes, we then induced expression of the *UAS-tCidA-tCidB* transgene with the germline specific driver *bam-Gal4*[42]. In testes dissected from *bam-Gal4>UAS-tCidA-tCidB* adult males, both effectors were first detected in *bam-Gal4* expressing cells (late spermatogonia/early spermatocytes) where they co-localized either on chromatin or in the cytoplasm (**Figure 2C,D**). Interestingly, tCidA and tCidB also localized in post-meiotic, early spermatid nuclei up until the onset of the histone-to-protamine transition (**Figure 2C**). The histone-to-protamine transition is a critical stage of spermiogenesis (the differentiation of spermatids into spermatozoa) which involves the massive replacement of histones with protamines in preparation of the final compaction of maturing spermatid nuclei and the acquisition of their needle-like nuclear shape[43]. Each germline cyst contains 64 spermatids with their nuclei organized into a tight bundle. Remarkably, while tCidA levels rapidly decreased in spermatid nuclei that were no longer packaged with histones, the tCidB signal remained intense in post-transition nuclei already packaged with protamines, until they reached a level of compaction that became incompatible with immunofluorescence (**Figure 2E**). Thus, although both factors have the ability to localize in early spermatid nuclei, only tCidB resists the global elimination of histones and accumulates in maturing sperm cells. To confirm this key observation, we tested another germline driver, *topi-Gal4,* which is only expressed in late spermatocytes[44]. Analysis of *topi-Gal4>UAS-tCidA-tCidB* testes revealed the very same differential distribution of Cid factors in spermatids (**Figure S2A**), indicating that their remarkable post-meiotic behavior is not influenced by their pre-meiotic expression pattern.

As previously reported[29], basal expression (without Gal4 activation) of the *UAS-tCidA-tCidB* transgene in males is sufficient to induce a full paternal-effect, CI-like phenotype at fertilization (**Table 1**). Analysis of these *+>UAS-tCidA-tCidB* testes revealed

that Cid factors were undetectable in pre-meiotic germ cells, confirming that their robust expression observed in previous experiments was entirely dependent on Gal4 activation. Remarkably however, a weak tCidB signal was nevertheless observed in late spermatid nuclei, at a stage that shows the brightest tCidB staining when using the *bam-Gal4* or *topi-Gal4* drivers (**Figure S2B**). We conclude that the level of effectors obtained from basal expression of the transgene remains generally below the sensitivity threshold of the microscope, except for late spermatid nuclei that accumulated sufficient amount of CidB. Taken together, our cytological analyses establish that CidA and CidB colocalize in male germ cells until the histone-to-protamine transition, a stage at which only CidB is eventually retained in maturing spermatid nuclei. These results thus strongly suggest that the presence of CidB, but not CidA, in sperm nuclei is critical to induce CI.

The *Wolbachia* CidB toxin is transmitted to the fertilized egg and associates with paternal DNA replication defects

To investigate the possible transmission of *Wolbachia* CI effectors to the egg via the sperm nucleus, *bam-Gal4>UAS-tCidA-tCidB* males were mated to wild-type, uninfected females and eggs were collected shortly after deposition. At fertilization, in *Drosophila*, protamines are rapidly removed from the needle-shape sperm nucleus and by the time the egg is laid, the partially decondensed male pronucleus has already reassembled its chromatin with maternally-provided histones[45,46]. As expected, none of the eggs fertilized by sperm from *bam-Gal4>UAS-tCidA-tCidB* males hatched (**Table 1**). Strikingly, in these eggs, the male pronucleus was systematically decorated with discrete nuclear foci of tCidB (100%, n=12) whereas none of the control eggs fertilized by *bam-Gal4>+* sperm were stained (0%, n=10). In clear contrast, tCidA remained undetectable above background level (**Figure 3A** and **Figure S3**). This result demonstrates that the

CidB toxin, but not the CidA antidote, is transmitted by the sperm nucleus to the egg, in full agreement with the prediction of the TA model[28].

To get insights about the possible consequences of CidB retention on paternal chromatin at fertilization, we first examined the removal of protamines from the decondensing male pronucleus. Indeed, it has been recently proposed that host chaperones involved in this critical step of male pronuclear formation could be targeted by CidB[36]. Co-staining tCidB with a protamine::EGFP[47] marker did not reveal any persisting protamine on these foci, suggesting that CidB does not interfere with protamine eviction, at least not to a detectable level (**Figure S4**). Note that previous cytological examinations of incompatible crosses in *Drosophila simulans* had also failed to detect persistent protamine on the male pronucleus at fertilization[11].

Embryos obtained from *bam-Gal4>UAS-tCidA-tCidB* fathers and observed during the first zygotic division all displayed a clear CI-like phenotype, with paternal chromosomes often forming a dense, unstructured chromatin mass. At this stage, tCidB was still detected on paternal chromatin in a majority of embryos (75%, n=20), where it was typically enriched in a single nuclear focus of unknown nature (**Figure 3B** and **Figure S3**). It was previously proposed that CI could result from catastrophic division of incompletely replicated paternal chromosomes at the first zygotic mitosis[10,11]. Remarkably, co-staining experiments of these CI-like embryos revealed the ectopic accumulation of the replication factor PCNA on paternal chromosomes during the first mitosis, particularly on tCidB-enriched foci, when these were present (68% of colocalization, n=19; **Figure 3C and Figure S5A-E**).

We then checked the distribution of Replication protein A (RpA), a single-stranded DNA binding protein complex which plays a critical role in the response to replication stress[48]. The RpA70-GFP[49] marker, which is normally only detected in replicating nuclei,

was found enriched on paternal chromatin throughout the first zygotic mitosis and showed a striking enrichment on tCidB foci, when these were present (100% of colocalization, n=14; **Figure 3D and Figure S6A-D**). Interestingly, co-expression of fCidB with mKate2::RpA3 in S2R+ cells also revealed an enrichment of RpA on fCidB nuclear foci (**Figure S6E**). These results suggest that the presence of CidB on chromatin prevents the normal progression of S phase, either by directly blocking DNA replication forks or by creating pre-replicative chromatin defects. In S2R+ cells, these putative unreplicated regions likely activate a replication checkpoint which could in turn lead to apoptosis. In contrast, early embryos lack S phase chekpoints[49] and incompletely replicated paternal chromosomes engage into catastrophic mitosis.

Although the molecular mechanism by which CidB could induce these replication defects remains to be established, we wanted to evaluate the role of the DUB domain in the CI-like phenotype. As already shown[29], we observed that a C1025A catalytic mutation in the *UAS-tCidA-tCidB* construct restores normal fertility to transgenic males. Surprisingly, however, induction of the *UAS-tCidA-tCidB*^{C1025A} mutant transgene with the *bam-Gal4* or *topi-Gal4* drivers led to an almost full male sterility (**Table 1**). Using the *bam-Gal4* driver, testis immunostainings revealed that the localization of tCidB^{C1025A} in early male germ cells was identical to what was previously observed with wild-type tCidB. However, tCidB^{C1025A} was barely detected in spermatid nuclei (**Figure 4**), suggesting that the DUB domain could play a role in the localization or stabilization of CidB in post-meiotic germ cells. Accordingly, examination of eggs fertilized by sperm from *bam-Gal4>UAS-tCidA-tCidB*^{C1025A} males failed to detect tCidB^{C1025A} on paternal chromosomes, with standard settings (n=15). By enhancing the corresponding color channel on confocal images, we nevertheless revealed a very faint signal just above background, suggesting a weak transmission of mutant CidB (**Figure S5G,H**). At the onset of the first division in

these zygotes, paternal chromosomes appeared mildly affected compared to the situation involving wild-type tCidB and did not show detectable replication stress with the PCNA marker (0%, n=10, **Figure S5F**). These chromosomes nevertheless formed a chromatin bridge at the end of the first division, resulting in the accumulation of aneuploid nuclei (**Figure 5**). These two phenotypic classes (Class I: strong defects followed by haploid divisions; Class II: mild-defects followed by chromatin bridges and aneuploid divisions) thus likely reflect the initial dose of toxin present in the male nucleus. We conclude that $CidB^{C1025A}$, although much less efficient in accumulating in spermatid nuclei than wild-type CidB, largely retains its capacity to perturb the division of paternal chromosomes after fertilization. These results are also consistent with the toxicity of the $CidB^{C1025A}$ and $CidB^{C1025R}$ DUB catalytic mutants in S2R+ cells. They also show that paternal transmission of very low to undetectable level of CidB is sufficient to induce a CI-like phenotype in *Drosophila*.

CidB is loaded in the sperm nuclei of naturally infected *Culex* mosquitoes

To validate the loading of CidB in insect sperm in a natural *Wolbachia* infection context, we raised a rabbit polyclonal antiserum against the $CidB^{wPip}$ protein (**Figure S7**) to perform immunofluorescence experiments on *Culex* testes. We first verified that the anti-CidB antibody recognized transgenic tCidB expressed in *bam-Gal4>UAS-tCidA-tCidB Drosophila* testes. Indeed, anti-CidB staining fully recapitulated the anti-Flag specific signal, including in maturing spermatid nuclei (**Figure 6A,B**).

We then used a *Culex* mosquito line (Slab)[50] naturally infected with *w*Pip as well as an uninfected version of this same line (Slab-TC), as a control. Immunostaining of Slab testes detected the presence of CidB in the nuclei of early germ cells while control, uninfected testes only showed non-specific staining (**Figure 6C**). Strikingly, CidB was abundantly detected in Slab spermatid nuclei, including elongating spermatid nuclei that

had progressed well beyond the histone-to-protamine transition (**Figure 6D**). These observations confirmed the general and remarkable capacity of the CidB toxin to be loaded in insect sperm nuclei to induce CI.

Discussion

The ability of CI-inducing *Wolbachia* strains to manipulate the fate of host embryos in a transgenerational manner is perhaps the most fascinating feature of Cytoplasmic Incompatibility. Since the link between *Wolbachia* and CI was first established in *Culex* mosquitoes 50 years ago[51], the mechanistic bases of this phenomenon has remained enigmatic. The early hypothesis that the genetic architecture of CI could rely on a pair of genes, a *mod* locus acting in the male germline to modify sperm and a *resc* locus controlling the rescue in eggs[24], has since been essentially validated by the recent discovery and functional characterization of CifA and CifB proteins. Still, the precise mechanism by which these molecular players operate in their host germ cells and zygote is still largely speculative without actually observing these proteins *in vivo*. By studying the cytological distribution and cellular impact of Cif proteins, our goal was to test and possibly refine current opposing models of CI. Our findings not only validate the Toxin-Antidote model but open new research avenues for the full elucidation of its molecular mechanism.

CidA associates with and neutralizes CidB *in vivo*

Our cytological observations of *w*Pip effectors in S2R+ and transgenic flies confirmed that CidA and CidB behave as a TA system, with CidA being critical to prevent CidB toxicity in proliferating cells. The co-localization of CidA and CidB in S2R+ as well as in somatic and germ cells is consistent with their direct binding *in vivo*, a conclusion also supported by recent structural resolution of CifA-CifB complexes[34]. We show that

these putative CidA-CidB heterodimers can localize either in the cytoplasm or in the nucleus, and in this case, were found associated with chromatin. Their co-expression had no detectable consequence on cell viability or normal progression of spermatogenesis, at least with the Gal4 drivers tested in this study. The constant association of CidA and CidB underlines the protective role of CidA against the deleterious effect of CidB, as shown in our experiments in S2R+ cells. Similarly, CidB immunodetection in infected *Culex* testes revealed that the protein is already present in early male germ cells, suggesting that *Wolbachia* does not restrict the expression of CI factors to a specific stage of spermatogenesis.

As discussed below, we demonstrate in this work that the DUB activity of CidB is not required for its toxicity in S2R+ cells nor in *Drosophila* eggs. In the light of this unexpected finding, the fact that CidB is still an active deubiquitylase when bound to $CidA^{29}$ is no longer at odds with the TA model. We conclude that CidB is harmless to *Drosophila* cells as long as it is physically associated with its cognate antidote.

CidB is specifically loaded in maturing spermatid nuclei

In contrast to the proliferative and meiotic phases of spermatogenesis, spermiogenesis and more specifically the histone-to-protamine transition marked a point of divergence in the CidA-CidB molecular partnership. We discovered that the predicted elimination of the antidote, which is a critical but unclear episode of the TA model, precisely occurs during this major chromatin reorganization event of *Drosophila* spermatogenesis. The mechanism by which CidB dissociates from CidA at the histone-to-protamine transition remains to be investigated. Our analysis of the $CidB^{C1025A}$ mutant indicates that CidB deubiquitylase activity contributes to maintain high amount of CidB in post-transition spermatids, perhaps by preventing CidB degradation by the testis-specific proteasome[52]. Activation of the mutant *UAS-tCidA-tCidB*^{C1025A} transgene with Gal4 seems

to compensate for the loss of CidB at the transition, thereby allowing sufficient amount of the toxin to be loaded in sperm nuclei for CI induction. In contrast, the basal expression of the wild-type transgene is sufficient to load a lethal dose of CidB in male gametes.

From a broader perspective, our work suggests that the histone-to-protamine transition, a process likely common to most insects, represents a universal window of opportunity for CifB effectors to associate with sperm chromatin until fertilization. This targeting mechanism also provides an explanation for the remarkable ability of a given pair of *Wolbachia* factors to induce CI in divergent host species, as illustrated here with CidA and CidB in *Drosophila* and *Culex*. As only CidB is retained in sperm nuclei, our study does not support any direct role of CidA^{wPip} in inducing CI, in apparent contradiction with the "Two-by-One" model proposed for *w*Mel Cifs expressed in *Drosophila*[26]. However, in the frame of the TA model, CidA could be required to safely escort and neutralize CidB until it reaches its final destination. As transgenic flies expressing CidB^{wPip} alone could not be established[29], the contribution of CidA in CI cannot be experimentally addressed. Recently, attempts to establish transgenic lines of *Anopheles gambiae* mosquitoes expressing only CidB^{wPip} also failed[35], thus indicating that the general toxicity of CidB is not restricted to *Drosophila*. However, in the same study, CidB transgenic males were occasionally obtained from crosses involving transgenic females with both CidA and CidB transgenes, suggesting that these individuals were allowed to develop thanks to the protective effect of maternal CidA. The fact that these CidB transgenic survivor males were capable of inducing strong CI in the absence of a CidA transgene seems to exclude a role of CidA. Conversely, overexpression of CidA in the *Anopheles* male germline lowered the penetrance of transgenic CI induced by CidB, suggesting that excess CidA could prevent the release of free CidB in spermatid nuclei. Thus, dosage of Cifs expression could

fine tune the balance between cellular toxicity and CI penetrance, in the context of the specific constraints imposed by the host.

Finally, it should also be mentioned that pioneer work of Beckmann & Fallon (2013)[53] originally identified CidA peptides in *Culex* spermathecae filled with sperm from infected males. Although the authors hypothesized that CidA was paternally-transmitted, the fact that females were also infected in this experiment leaves open the possibility of a maternal origin of CidA, as previously noted[5]. Development of anti-CidA antibodies should help clarifying this point in future work.

Transmission of the CidB toxin at fertilization

Paternal transmission of CidB to the fertilized egg is a central prediction of the TA model, which is now validated. Once loaded in spermatid nuclei and separated from CidA, the unleashed CidB toxin does not seem to affect sperm integrity in a detectable manner until fertilization. Despite its ultracompact structure, insect sperm chromatin is relatively plastic. For instance, it can accommodate large fluorescent-tagged protamines without detectable perturbation[47]. Although Gal4 activation of the *UAS-tCidA-tCidB* transgene in *Drosophila* testes apparently yielded high levels of tCidB in spermatid nuclei, staining spermatids from infected *Culex* with the same antibody gave similar signal intensity. It is thus reasonable to think that the amount of CidB transmitted by *Culex* sperm is comparable to what we observed with *Drosophila* transgenic males.

In this study, we also provide evidence that CidB remains tightly associated with the male pronucleus at fertilization during the rapid replacement of protamines with histones. The stable association of CidB with the paternal genome during this massive chromatin remodeling event suggests a robust interaction of the toxin with sperm DNA, in a direct or indirect manner. In contrast to the homogeneous nuclear distribution of CidA and CidB in somatic or early germ cell nuclei, CidB frequently showed a highly

heterogeneous distribution in the male pronucleus, with a preference for a few nuclear foci. This change in nuclear distribution of free CidB suggests that its ability to firmly establish its deadly interaction with chromatin is blocked by its physical association with CidA. We propose that this simple principle is at the heart of the "rescue" mechanism of compatible eggs by CidA, which constitutes the final prediction of the TA model of CI.

As our results indicate that CidB toxicity likely functions by impeding DNA replication (as discussed below), this leaves time for CidA to bind and neutralize CidB during the decompaction of the male pronucleus before any damage is done. Indeed, S phase begins only at the end of pronuclear migration, when the male pronucleus is already decondensed[54]. In compatible crosses, we predict that maternal CidA should be present throughout the egg cytoplasm before fertilization, like egg proteins in charge of removing protamines, for instance[46]. Expression analysis of *Wolbachia* genes in infected flies have actually revealed that CifA is expressed at much higher level than CifB in ovaries[31]. Free cytoplasmic CidA could bind paternal CidB on sperm chromatin at fertilization and neutralize it before DNA replication. Unfortunately, although the *UAS-tCidA-tCidB* transgene proved very useful in this study, this genetic tool could not be used to study the "rescue" mechanism of CI, as previously reported[29]. However, the study in *Anopheles* has shown that transgenic CI induced by CidB^{wPip} could be successfully rescued using a strong maternal CidA transgene[35]. The lack of rescue in *Drosophila* transgenics could thus result from inappropriate expression of CidA in the female germline, a possibility that needs to be tested in future work. In addition, focusing on another pair of effectors with efficient rescue, such as the *w*Mel CifA and CifB[26], will help understanding the neutralization mechanism at fertilization, and could uncover potential differences between *Wolbachia* strains.

CidB and the poisoning of paternal DNA replication

At the onset of the first zygotic mitosis, we frequently observed CidB accumulating on a single paternal nuclear region. As spectacular and intriguing this result is, it is important to keep in mind that *w*Pip and its effectors did not co-evolve in association with the *Drosophila* genome but with the *Culex* genome. We ignore the identity of this region and if it represents a bona fide genomic target of CidB that could be common to both insect genomes. In any case, the association of this CidB enriched nuclear region with PCNA and RpA70 markers allowed us to establish a link between the presence of the toxin on the paternal genome and defective progression of DNA replication. We made two additional observations that, we think, are important to understand CidB toxicity. First, not all zygotes display the CidB enriched chromatin region but all engage into a catastrophic first division typical of CI embryos. Second, very low, basal expression of the *UAS-tCidA-tCidB* transgene induced a full CI-like phenotype. Altogether, these results indicate that $CidB^{wPip}$ is an efficient toxin that kills *Drosophila* zygotes at very low dosage. We hypothesize that CidB, through its association or proximity with DNA, could directly or indirectly block the progression of the replisome, leading to defective DNA replication. Such a poisoning mechanism is not unknow in the bacterial Toxin-Antidote world. In fact, the classical *Escherichia coli* addiction toxin CcdB poisons the GyrA catalytic subunit of gyrase, a topoisomerase involved in disentangling DNA during replication. As a result, the poisoned enzyme is trapped as a covalent adduct on DNA and blocks DNA polymerases[38,55]. If CidB indeed poisons DNA replication through a similar mechanism, a single roadblock on DNA could be theoretically sufficient to jeopardize the timely replication of the paternal genome but would remain undetectable in microscopy. The phenotypic defects observed in Class II CI-like embryos shown in **Figure 5** are compatible with this low dose poisoning. Alternative toxic effects models are possible, such as an earlier perturbation of pronuclear chromatin by CidB that would in turn affect DNA

replication. In any case, the CidB target should be at least common to *Drosophila* zygotes and S2R+ cells, making the recently proposed hypothesis that CidB could target protamine-histone exchange factors[36] rather unlikely, in our opinion. Using *w*Mel Cifs transgenes, these authors reported a weak CI-rescuing effect by maternal overexpression of the nuclear import protein Kap-α2 and the protamine chaperone P32. However, increasing nucleocytoplasmic trafficking and protamine removal activity might putatively result in more efficient elimination of CidB from the male pronucleus. Future work should aim at determining the structural bases of CidB interaction with chromatin and the precise mechanism involved in its nuclear toxicity.

Acknowledgments

We thank John Beckmann, Marc Hochstrasser, Mia Levine, Anne Royou and Jean-Louis Couderc for fly stocks and plasmids. We also thank Marie Delattre, Raphaëlle Dubruille and Guillermo Orsi for critical reading of the manuscript. We are grateful to the Bloomington Drosophila Stock Center and the Drosophila Genomics Resource Center at Indiana university for fly stocks and plasmids. We acknowledge the contribution of Lyon SFR Biosciences (UAR3444/CNRS, US8/INSERM, ENS de Lyon, UCBL) imaging facility (PLATIM) and fly food production (Arthrotools). We also acknowledge the imaging facility MRI, member of the national infrastructure France-BioImaging infrastructure supported by the French National Research Agency (ANR-10-INBS-04, «Investments for the future»). This work was supported by a French National Research Agency (ANR) grant ("CIAWOL" ANR-16- CE02-0006-01) to FL, BL and MS, a MUSE program of the University of Montpellier (AAP17REC-FRS04-GENEWOL) to FL and a grant from the Fondation Schlumberger pour l'Education et la Recherche (FSER), FSER202002011118 to FL.

Author contributions

Conceptualization: BH, FL, MS, BL

Investigation: BH, KT, AG, HS, FL, BL

Visualization: KT, FL, BL

Funding acquisition: FL, BL, MS

Supervision: FL, MS, BL

Writing – original draft: BL

Writing – review & editing: BH, KT, AG, MS, FL, BL

Declaration of interests

The authors declare no competing interests.

References

1. Werren, J.H., Baldo, L., and Clark, M.E. (2008). Wolbachia: master manipulators of invertebrate biology. Nat. Rev. Microbiol. *6*, 741–751.

2. Landmann, F. (2019). The Wolbachia Endosymbionts. Microbiol Spectr *7*, BAI-0018-2019.

3. Hertig, M and Wolbach, S.B. (1924). Studies on Rickettsia-like micro-organisms in insects. J Med Res *44*, 329–374.

4. Laven, H (1956). Cytoplasmic inheritance in Culex. Nature *177*, 141–42.

5. Shropshire, J.D., Leigh, B., and Bordenstein, S.R. (2020). Symbiont-mediated cytoplasmic incompatibility: What have we learned in 50 years? eLife *9*, e61989.

6. Turelli, M., and Hoffmann, A.A. (1991). Rapid spread of an inherited incompatibility factor in California Drosophila. Nature *353*, 440–442.

7. Utarini, A., Indriani, C., Ahmad, R.A., Tantowijoyo, W., Arguni, E., Ansari, M.R., Supriyati, E., Wardana, D.S., Meitika, Y., Ernesia, I., et al. (2021). Efficacy of Wolbachia-Infected Mosquito Deployments for the Control of Dengue. N. Engl. J. Med. *384*, 2177–2186.

8. Callaini, G., Dallai, R., and Riparbelli, M.G. (1997). Wolbachia-induced delay of paternal chromatin condensation does not prevent maternal chromosomes from entering anaphase in incompatible crosses of Drosophila simulans. J. Cell Sci. *110*, 271–280.

9. O'Neill, S.L., and Karr, T.L. (1990). Bidirectional incompatibility between conspecific populations of Drosophila simulans. Nature *348*, 178–180.

10. Tram, U., and Sullivan, W. (2002). Role of Delayed Nuclear Envelope Breakdown and Mitosis in *Wolbachia* -Induced Cytoplasmic Incompatibility. Science *296*, 1124–1126.

11. Landmann, F., Orsi, G.A., Loppin, B., and Sullivan, W. (2009). Wolbachia-Mediated Cytoplasmic Incompatibility Is Associated with Impaired Histone Deposition in the Male Pronucleus. PLoS Pathog. *5*, e1000343.

12. Tram, U., Fredrick, K., Werren, J.H., and Sullivan, W. (2006). Paternal chromosome segregation during the first mitotic division determines *Wolbachia* -induced cytoplasmic incompatibility phenotype. J. Cell Sci. *119*, 3655–3663.

13. Poinsot, D., Bourtzis, K., Markakis, G., Savakis, C., and Merçot, H. (1998). Wolbachia Transfer from Drosophila melanogaster into D. simulans: Host Effect and Cytoplasmic Incompatibility Relationships. Genetics *150*, 227–237.

14. Bonneau, M., Landmann, F., Labbé, P., Justy, F., Weill, M., and Sicard, M. (2018). The cellular phenotype of cytoplasmic incompatibility in Culex pipiens in the light of cidB diversity. PLOS Pathog. *14*, e1007364.

15. Lassy, C.W., and Karr, T.L. (1996). Cytological analysis of fertilization and early embryonic development in incompatible crosses of Drosophila simulans. Mech. Dev. *57*, 47–58.

16. Zhou, X.-F., and Li, Z.-X. (2016). Establishment of the cytoplasmic incompatibility-inducing Wolbachia strain wMel in an important agricultural pest insect. Sci. Rep. *6*, 39200.

17. Ross, P.A., Gu, X., Robinson, K.L., Yang, Q., Cottingham, E., Zhang, Y., Yeap, H.L., Xu, X., Endersby-Harshman, N.M., and Hoffmann, A.A. (2021). A wAlbB Wolbachia Transinfection Displays Stable Phenotypic Effects across Divergent Aedes aegypti Mosquito Backgrounds. Appl. Environ. Microbiol. *87*, e01264-21.

18. Clark, M.E., Heath, B.D., Anderson, C.L., and Karr, T.L. (2006). Induced Paternal Effects

523 Mimic Cytoplasmic Incompatibility in Drosophila. Genetics *173*, 727–734.
524 19. Zheng, Y., Ren, P.-P., Wang, J.-L., and Wang, Y.-F. (2011). Wolbachia-Induced Cytoplasmic
525 Incompatibility Is Associated with Decreased Hira Expression in Male Drosophila. PLoS ONE *6*,
526 e19512.
527 20. Liu, C., Wang, J.-L., Zheng, Y., Xiong, E.-J., Li, J.-J., Yuan, L.-L., Yu, X.-Q., and Wang, Y.-
528 F. (2014). Wolbachia-induced paternal defect in Drosophila is likely by interaction with the juvenile
529 hormone pathway. Insect Biochem. Mol. Biol. *49*, 49–58.
530 21. Pontier, S.M., and Schweisguth, F. (2015). A Wolbachia-Sensitive Communication between
531 Male and Female Pupae Controls Gamete Compatibility in Drosophila. Curr. Biol. *25*, 2339–2348.
532 22. Jacquet, A., Horard, B., and Loppin, B. (2017). Does pupal communication influence
533 Wolbachia -mediated cytoplasmic incompatibility? Curr. Biol. *27*, R53–R55.
534 23. Hurst, L.D. (1991). The evolution of cytoplasmic incompatibility or when spite can be
535 successful. J. Theor. Biol. *148*, 269–277.
536 24. Werren, J.H. (1997). Biology of *Wolbachia*. Annu. Rev. Entomol. *42*, 587–609.
537 25. Poinsot, D., Charlat, S., and Merçot, H. (2003). On the mechanism of *Wolbachia* -induced
538 cytoplasmic incompatibility: Confronting the models with the facts: Problems and paradigms.
539 BioEssays *25*, 259–265.
540 26. Shropshire, J.D., and Bordenstein, S.R. (2019). Two-By-One model of cytoplasmic
541 incompatibility: Synthetic recapitulation by transgenic expression of cifA and cifB in Drosophila.
542 PLOS Genet. *15*, e1008221.
543 27. Chen, H., Zhang, M., and Hochstrasser, M. (2020). The Biochemistry of Cytoplasmic
544 Incompatibility Caused by Endosymbiotic Bacteria. Genes *11*, 852.
545 28. Beckmann, J.F., Bonneau, M., Chen, H., Hochstrasser, M., Poinsot, D., Merçot, H., Weill, M.,
546 Sicard, M., and Charlat, S. (2019). The Toxin–Antidote Model of Cytoplasmic Incompatibility:
547 Genetics and Evolutionary Implications. Trends Genet. *35*, 175–185.
548 29. Beckmann, J.F., Ronau, J.A., and Hochstrasser, M. (2017). A Wolbachia deubiquitylating
549 enzyme induces cytoplasmic incompatibility. Nat. Microbiol. *2*, 17007.
550 30. LePage, D.P., Metcalf, J.A., Bordenstein, S.R., On, J., Perlmutter, J.I., Shropshire, J.D.,

Layton, E.M., Funkhouser-Jones, L.J., Beckmann, J.F., and Bordenstein, S.R. (2017). Prophage WO genes recapitulate and enhance Wolbachia-induced cytoplasmic incompatibility. Nature *543*, 243–247.

31. Lindsey, A.R.I., Rice, D.W., Bordenstein, S.R., Brooks, A.W., Bordenstein, S.R., and Newton, I.L.G. (2018). Evolutionary Genetics of Cytoplasmic Incompatibility Genes cifA and cifB in Prophage WO of Wolbachia. Genome Biol. Evol. *10*, 434–451.

32. Shropshire, J.D., Kalra, M., and Bordenstein, S.R. (2020). Evolution-guided mutagenesis of the cytoplasmic incompatibility proteins: Identifying CifA's complex functional repertoire and new essential regions in CifB. PLOS Pathog. *16*, e1008794.

33. Shropshire, J.D., Rosenberg, R., and Bordenstein, S.R. (2021). The impacts of cytoplasmic incompatibility factor (*cifA* and *cifB*) genetic variation on phenotypes. Genetics *217*, 1–13.

34. Xiao, Y., Chen, H., Wang, H., Zhang, M., Chen, X., Berk, J.M., Zhang, L., Wei, Y., Li, W., Cui, W., et al. (2021). Structural and mechanistic insights into the complexes formed by *Wolbachia* cytoplasmic incompatibility factors. Proc. Natl. Acad. Sci. *118*, e2107699118.

35. Adams, K.L., Abernathy, D.G., Willett, B.C., Selland, E.K., Itoe, M.A., and Catteruccia, F. (2021). Wolbachia cifB induces cytoplasmic incompatibility in the malaria mosquito vector. Nat. Microbiol. *6*, 1575–1582.

36. Beckmann, J.F., Sharma, G.D., Mendez, L., Chen, H., and Hochstrasser, M. (2019). The Wolbachia cytoplasmic incompatibility enzyme CidB targets nuclear import and protamine-histone exchange factors. eLife *8*, e50026.

37. Riffaud, C., Pinel-Marie, M.-L., and Felden, B. (2020). Cross-Regulations between Bacterial Toxin–Antitoxin Systems: Evidence of an Interconnected Regulatory Network? Trends Microbiol. *28*, 851–866.

38. Burga, A., Ben-David, E., and Kruglyak, L. (2020). Toxin-Antidote Elements Across the Tree of Life. Annu. Rev. Genet. *54*, 387–415.

39. Morrow, M.E., Morgan, M.T., Clerici, M., Growkova, K., Yan, M., Komander, D., Sixma, T.K., Simicek, M., and Wolberger, C. (2018). Active site alanine mutations convert deubiquitinases into high- affinity ubiquitin- binding proteins. EMBO Rep. *19*, e45690.

40. Diao, F., and White, B.H. (2012). A Novel Approach for Directing Transgene Expression in

Drosophila : T2A-Gal4 In-Frame Fusion. Genetics *190*, 1139–1144.

41. Cherbas, L., Hu, X., Zhimulev, I., Belyaeva, E., and Cherbas, P. (2003). EcR isoforms in *Drosophila* : testing tissue-specific requirements by targeted blockade and rescue. Development *130*, 271–284.

42. Chen, D., and McKearin, D.M. (2003). A discrete transcriptional silencer in the *bam* gene determines asymmetric division of the *Drosophila* germline stem cell. Development *130*, 1159–1170.

43. Hao, S.-L., Ni, F.-D., and Yang, W.-X. (2019). The dynamics and regulation of chromatin remodeling during spermiogenesis. Gene *706*, 201–210.

44. Raychaudhuri, N., Dubruille, R., Orsi, G.A., Bagheri, H.C., Loppin, B., and Lehner, C.F. (2012). Transgenerational Propagation and Quantitative Maintenance of Paternal Centromeres Depends on Cid/Cenp-A Presence in Drosophila Sperm. PLoS Biol. *10*, e1001434.

45. Loppin, B., Bonnefoy, E., Anselme, C., Laurençon, A., Karr, T.L., and Couble, P. (2005). The histone H3.3 chaperone HIRA is essential for chromatin assembly in the male pronucleus. Nature *437*, 1386–1390.

46. Tirmarche, S., Kimura, S., Dubruille, R., Horard, B., and Loppin, B. (2016). Unlocking sperm chromatin at fertilization requires a dedicated egg thioredoxin in Drosophila. Nat. Commun. *7*, 13539.

47. Raja, S.J., and Renkawitz-Pohl, R. (2005). Replacement by Drosophila melanogaster Protamines and Mst77F of Histones during Chromatin Condensation in Late Spermatids and Role of Sesame in the Removal of These Proteins from the Male Pronucleus. Mol Cell Biol *25*, 6165–6177.

48. Nguyen, D.-D., Kim, E.Y., Sang, P.B., and Chai, W. (2020). Roles of OB-Fold Proteins in Replication Stress. Front. Cell Dev. Biol. *8*, 574466.

49. Blythe, S.A., and Wieschaus, E.F. (2015). Zygotic Genome Activation Triggers the DNA Replication Checkpoint at the Midblastula Transition. Cell *160*, 1169–1181.

50. Georghiou, G.P., Metcalf, I.R.L., and Gidden, F.E. (1966). Carbamate-Resistance in Mosquitos. Bull Wld Hlth Org *35*, 691–708.

51. Yen, J.H., and Barr, A.R. (1971). New Hypothesis of the Cause of Cytoplasmic Incompatibility in Culex pipiens L. Nature *232*, 657–658.

52. Zhong, L., and Belote, J.M. (2007). The testis-specific proteasome subunit Prosα6T of *D.*

melanogaster is required for individualization and nuclear maturation during spermatogenesis. Development *134*, 3517–3525.

53. Beckmann, J.F., and Fallon, A.M. (2013). Detection of the Wolbachia protein WPIP0282 in mosquito spermathecae: Implications for cytoplasmic incompatibility. Insect Biochem. Mol. Biol. *43*, 867–878.

54. Loppin, B., Dubruille, R., and Horard, B. (2015). The intimate genetics of *Drosophila* fertilization. Open Biol. *5*, 150076.

55. Dao-Thi, M.-H., Van Melderen, L., De Genst, E., Afif, H., Buts, L., Wyns, L., and Loris, R. (2005). Molecular Basis of Gyrase Poisoning by the Addiction Toxin CcdB. J. Mol. Biol. *348*, 1091–1102.

56. O'Neill, S.L., Giordano, R., Colbert, A.M., Karr, T.L., and Robertson, H.M. (1992). 16S rRNA phylogenetic analysis of the bacterial endosymbionts associated with cytoplasmic incompatibility in insects. Proc. Natl. Acad. Sci. *89*, 2699–2702.

57. Bonneau, M., Caputo, B., Ligier, A., Caparros, R., Unal, S., Perriat- Sanguinet, M., Arnoldi, D., Sicard, M., and Weill, M. (2019). Variation in *Wolbachia cidB* gene, but not *cidA* , is associated with cytoplasmic incompatibility *mod* phenotype diversity in *Culex pipiens*. Mol. Ecol. *28*, 4725–4736.

FIGURE LEGENDS

Figure 1. Cid effectors behave as a toxin-antidote system in *Drosophila* S2R+ cells

(A) Distribution of fluorescent fCidA and fCidB effectors in S2R+ cells transfected with the indicated DNA construct. T2A is a self-cleaving peptide. Bar: 10 µm.

(B) Cell viability assayed by flow cytometry. Growth of transfected cells is represented as a log2 fold change of the fraction of transfected cells between day 2 and 4 post-transfection. Middle bar are mean values from 3 independent experiments, error bars are SD. Asterisk indicates a P value <0.01. See also Figure S1, Video S1, S2.

Figure 2. CidB localizes to maturing sperm nuclei in *Drosophila* transgenic testes

(A) Scheme illustrating the UAS/Gal4 system in *Drosophila*.

(B) Distribution of tCid effectors in the nuclei (left) or cytoplasm (right) of larval salivary gland cells. Bar: 20µm.

(C) Distribution of tCid effectors in *bam-Gal4>UAS-tCidA-tCidB* and in control *bam-Gal4>+* testes. The effectors colocalize in early germ cell nuclei in the apical region of the testis (inset, left). After meiosis (inset, right), both effectors are detected in early spermatid nuclei packaged with histones (arrow) but V5::CidA progressively disappears from spermatid nuclei bundles after the histone-to-protamine transition (arrowhead). The control testis (right panels) shows background staining for anti-Flag and anti-V5 antibodies.

(D) Another *bam-Gal4>UAS-tCidA-tCidB* testis where both effectors are mainly localized in the cytoplasm of early germ cells. In spermatids, however, their distribution is identical to the previous example.

(E) Flag::CidB is retained in spermatid nuclei packaged with protamines, here detected with a ProtamineB::EGFP (ProtB::EGFP) transgene (arrowhead).

Histones in (C) and (D) are revealed with and anti-acetylated H4 (H4ac) antibody. Note that spermatid nuclei in some ProtB::EGFP positive cysts are too compact for antibody penetration. Bars: 20µm. See also Figure S2.

Figure 3. CidB is transmitted to the egg and associates with paternal chromosomes

(A) In eggs fertilized by a sperm from a *bam-Gal4>UAS-tCidA-tCidB* male, Flag::CidB, but not V5::CidA, is specifically detected in the male pronucleus as multiple foci. PB: polar bodies. Pronuclei are indicated with symbols. Flag staining is not detected in a male pronucleus in a control egg (right panels).

(B) Flag::CidB is retained on the abnormally organized paternal chromatin mass during the first zygotic division in a CI-like embryo. Note the prominent accumulation of tCidB in a single nuclear focus (arrow). Right panels: control embryos at the same stages.
(C) Flag::CidB colocalizes with ectopic PCNA on paternal chromatin in a CI-like embryo.
(D) Flag::CidB colocalizes with the replication stress marker RpA::GFP (arrow).
Control eggs and embryos are from a *bam-Gal4>+* X WT cross. Note the weak, non-specific anti-V5 staining on paternal chromatin, which is identified with the H4ac marker. Bar: 5µm. See also Figure S3-S6.

Figure 4 - Distribution of tCid effectors in *bam-Gal4>UAS-tCidA-tCidB^{C1025A}* testes

Confocal images of testes stained for Flag::CidB^{C1025A}, V5::CidA and acetylated H4 (H4ac). In *bam-Gal4>UAS-tCidA-tCidB^{C1025A}* males, both effectors are first detected in early germ cells corresponding to the *bam* expression domain (arrow in top right panels). After meiosis (bottom panels), V5::CidA is no longer detected above background level and Flag::CidB^{C1025A} is only detected at low level in post-transition spermatids (arrowhead). Bars: 20 µm.

Figure 5 - The *UAS-tCidA-tCidB* and *UAS-tCidA-tCidB^{C1025A}* transgenes induce distinct CI phenotypes

(A) Cycle 1 embryos stained for DNA (blue) and H4ac (white). Two CI-like phenotypic classes are distinguished in these embryos. In Class I CI, paternal chromatin (indicated by a male symbol) forms a relatively dense mass that remains separated from maternally derived-nuclei. In Class II CI, paternal chromatin is less severely affected and paternal chromosomes (arrows) attempt to divide in anaphase.

(B) Cycle 2 embryos stained as above. In Class I, paternal chromatin remains separated from the two maternally-derived nuclei. In Class II, chromatin bridges and fragmented chromosomes (arrows) of presumably paternal origin are observed.

(C) Cycle 3 embryos. In Class I, four haploid nuclei are visible and paternal chromatin remains separated. In Class II, aneuploid embryos with chromatin bridges and fragmented chromosomes (arrows) are observed. Bar: 5µm.

(D) Quantification of WT, Class I and Class II phenotypes in cycle 1-3 embryos fertilized by fathers of indicated genotype. n: number of embryos scored for each nuclear cycle. Note that for nuclear cycle 1, only embryos in anaphase or telophase were scored as phenotypic differences are more obvious at these phases.

Figure 6. CidB localizes in maturing sperm nuclei in *Wolbachia*-infected *Culex* testes

(A) Anti-CidB staining on *bam-Gal4>UAS-tCidA-tCidB Drosophila* testes with nuclear (top) or cytoplasmic (bottom) localization of CidB. Note that the anti-CidB and anti-Flag stainings are indistinguishable.

(B) Same as in (A), but showing the spermatid bundles. Note the non-specific staining of the sperm flagella region with the anti-Flag antibody.

(C) An infected *Culex* Slab testis showing accumulation of CidB in early male germ cell nuclei (arrow in left inset). CidB is detected in spermatid nuclei still packaged with histones (arrow, middle inset) as well as in elongated, post-transition spermatid nuclei (arrowhead, middle and right panels). Note that some spermatid nuclei in right panel are too compact for antibody penetration.

(D) An uninfected SlabTC testis stained as in (A). Note that a few somatic nuclei show a non-specific anti-CidB staining. Bar: 20µm. See also Figure S7.

STAR Methods

Resource Availability

Lead contact

Further information and requests for resources and reagents should be directed to and will be fulfilled by the lead contact, Benjamin Loppin (benjamin.loppin@ens-lyon.fr).

Materials availability

Materials generated in this study are available upon request from the lead contact.

Data and code availability

This study did not generate any unique datasets or code.

Experimental Model Details

Drosophila S2R+ cell lines

S2R+ cells were obtained from the Drosophila Genomics Resource Center (DGRC) and cultured in Schneider's Drosophila medium (Dutscher #L0207-500) supplemented with 10% Fetal Bovine Serum (Dutscher #S1810-500) at 25°C.

Drosophila strains

Flies were reared at 25°C on a standard agar, yeast and cornmeal fly medium supplemented with propionic acid.

Culex strains

Culex quinquefasciatus Slab line was originally founded with individuals sampled in California, USA[50]. We used an isofemale line maintained in insectary conditions in Montpellier (at 25 ± 2 °C and 75 ± 2% relative humidity and a 12:12 hours photoperiod). Larvae are fed with 10g/L of a mixture containing 25% of shrimp powder (fish meal, krill meal, wheat gluten, squid meal, fish oil, pea starch, pea protein, yeast) and 75% of rabbit pellets (wheat bran, compacted dehydrated alfalfa, sunflower seed cake, cane molasses, beet

pulp, calcium carbonate). Adults are kept in 65 dm3 cages and fed with a honey solution (20g/L solution). Females are fed weekly with turkey blood in heparin sodium using a Hemotek membrane feeding system (Discovery Workshops, UK). To obtain the control Slab-TC line without *Wolbachia*, Slab larvae were treated with tetracycline (50 mL/L for larval treatment using a 0.4g/L solution) for 3 generations.

Method Details

Plasmid constructs for expression of fluorescent Cids in *Drosophila* S2R+ cells

pAct5C-mkate2-CidA-T2A-sfGFP-CidB

A synthetic cassette (Genescript) containing the mkate2-T2A-sfGFP bloc was inserted in the Multiple Cloning Site of a *Drosophila* cell vector based on the pMT-V5-HisC (Invitrogen #V412020) modified to have an Actin5C (Act5C) promoter. The *CidA* gene was derived from the pUASP-6His-V5-CidA-T2A-Flag-CidB-attP plasmid[29] and was fused to the C-terminus of the mkate2 red fluorescent protein. The *CidB* gene was made of synthetic fragments obtained from Genescript (details available upon request) and was fused to the C-terminus of superfolder GFP (sfGFP). The 73 bp third intron of *D. melanogaster nanos (nos)* gene was inserted in the 5' end of *CidB* to introduce a frameshift and avoid toxic leakage expression in *E. coli*.

pAct5C-mkate2-CidA-T2A-sfGFP-CidB^{C1025A}

The C1025A and C1025R *CidB* mutations were created with the Q5 directed mutagenesis kit (NEB # E0554S). All plasmids were obtained by Gibson cloning using the NEBuilder Hifi DNA Assembly kit (NEB #E5520S) and verified by Sanger sequencing. Fragments were created by PCR with the Q5 polymerase (NEB #M0491S). Transgenes were codon optimized for expression in *D. melanogaster* cells.

pAct5C-mkate2-RPA3-T2A-sfGFP-CidB

The *RPA3* gene coding sequence was kindly provided by Dr. Anne Royou and fused by Gibson to the the C-terminus of mkate2 in our construct.

Drosophila cell culture, transfection and imaging

For live microscopy, cells were plated in 35 mm glass bottom dishes (Cellvis #D35-20-1.5-N) and transfected with Lipofectamine 3000 (Invitrogen #L3000008) and 500 ng of purified plasmid DNA, according to manufacturer's instructions. Transfected cells were observed between 24 and 48 hours after transfection. Confocal imaging was performed with a Leica SP5-SMD microscope equipped with a 63X 1.4 NA objective lens. Time-lapse videos S1 and S2 were acquired with a Andor Dragonfly spinning disk equipped with a 60X Plan Apo lambda 1.4 NA objective lens.

For immunofluorescence, S2R+ cells were cultured on coverslips in 12-well plates and transfected as above. Cells were fixed at 3-days post transfection with 4% paraformaldehyde (PFA) for 20 min at room temperature, then permeabilized 30 min with 0.5% Triton X-100 (Sigma-Aldrich) and blocked 1 hour with 1% Bovine Serum Albumin (BSA, Sigma-Aldrich) diluted in PBS. Cells were subsequently incubated 1 hour with purified anti-CidB^{wPip} antibody (1:200), washed in PBS, then incubated 1 hour with an anti-rabbit Alexa Fluor^{TM} 633-conjugated secondary antibody (1:500; Invitrogen, #A21070). Both antibodies were diluted in PBS containing 0.2% BSA. Finally, cells were incubated 5 minutes with Hoechst 33342 (1:10,000; Thermo Scientific™, #62249) to label nuclei. Coverslips were mounted in Dako mounting medium (Agilent, #S3023). Images were acquired using a 63X 1.4 NA Plan-Apochromat Oil PH3 objective on a Zeiss AxioImager Z2/Apotome microscope and a Zeiss ApoTome-slider introduced into the field-stop plane of the microscope to improve image resolution. We used ZEN software to operate the microscope. All images were acquired with a CMOS Orca Flash 4.0 B&W camera and processed with the Image J software.

Drosophila cell viability assay

Transient transfections were performed with the constructs and method described above, to assess the toxicity induced by the fCid effectors by flow cytometry. Analyses were carried out with 3 independent experiments and technical triplicates. For each replicate, S2R+ cells from a single 25 cm^2 culture flask were plated in two wells of a 12-well plate and transfected with 500 ng of plasmid DNA. To limit late transfection events, medium was replaced the following day. For each time-point analysed, the cell content of one well was processed as follows: cells were washed once then detached by pipetting in 500 µl PBS, and immediately analysed by flow cytometry on a sampling of 200,000 counted events. Data acquisition was performed with a Novocyte ACEA cytometer and analysis performed with the NovoExpress (ACEA) software. For single fCidA or fCidB transgene constructs, only the relevant fluorescent signal was used to detect transfected cells.

Drosophila stocks

The transgenic stocks *y w; pUASP-6His-V5-CidA-T2A-Flag-CidB-attP/+* and *y w; pUASP-6His-V5-CidA-T2A-Flag-CidB^{C1025A}-attP*[29], inserted in the *PBac{y[+]-attP-9A}VK00027* platform on chromosome 3R (89E11), were kindly provided by J.F. Beckmann. Adult virgin females from these stocks were crossed with the appropriate Gal4 driver males and F1 adult males or larvae carrying both transgenes were analyzed. The genotype of *+>UAS-tCidA-tCidB* males is: *y w/Y; pUASP-6His-V5-CidA-T2A-Flag-CidB-attP/+*. *Sevelin* is a wild-type *D. melanogaster* stock obtained from Mia Levine. The *bam-Gal4* driver is a third chromosome insertion of *P{w[+mC]=bam-GAL4:VP16}*[42] and is a gift from J.L. Couderc. Additional stocks are: *w; P{w[+mC]=protamineB-eGFP}*[47], *w; P{w[+mC]=RPA70-GFP}attP2*[49], *w; M{RFP[3xP3.PB] w[+mC]=topi-GAL4.VP16}ZH-86Fb/TM3, Ser[1]* (*topi-Gal4*, Bloomington Drosophila Stock Center #91776)[44] and *w; P{w[+mC]=Sgs3-GAL4.PD}TP1* (*Sgs3-Gal4*, Bloomington Drosophila Stock Center #6870)[41]. All stocks were checked for the

absence of *Wolbachia* infection by fluorescent microscopy and PCR detection of 16S rRNA[56]. Drosophila stocks are listed in the Key Ressources table.

Drosophila **fertility tests**

Virgin *UAS-tCidA-tCidB* /+ or *UAS-tCidA-tCidB*^{C1025A} *females* were mass crossed with transgenic Gal4 males at 25°C and males heterozygous for both the driver and the UAS transgene were recovered in the F1 progeny.

To measure fertility, fifteen 0 to 48-hour-old virgin females were aged for 2 additional days at 25°C in presence of fifteen 2 to 4-day-old males of the genotype of interest. Females were then allowed to lay eggs on grape-juice agar plates for 12 hours. Embryos were counted and then let to develop for at least 36 hours at 25°C. Unhatched embryos were counted over four consecutive days to determine hatching rates.

Immunofluorescence and imaging of ***Drosophila*** **tissues and embryos**

Drosophila testes

Testes from 2 to 4-day-old males were dissected in PBS-T (PBS 1X with 0.15% Triton X-100) and fixed for 20 min in 4% PFA at room temperature. Testes were washed 3 times in PBS-T and incubated with primary antibody overnight at 4°C. After three 20 minutes washes in PBS-T, they were incubated with secondary antibodies at room temperature for 2 hours. Testes were then mounted in Dako mounting medium (Agilent, #S3023) containing 1 µg/ml DAPI.

Drosophila salivary glands

Salivary glands from late third instar larvae were dissected in PBS-T and fixed at room temperature in 4% PFA in PBS-T for 20 minutes. Immunofluorescence and mounting were performed as for testes.

Drosophila embryos

About fifty pairs of 1 to 4-day-old adults were mass crossed and allowed to mate for two days before embryo collection. Early (0-30 minutes) embryos were collected on grape juice agar-

agar plates, immediately dechorionated in bleach, fixed in a 1:1 heptane:methanol mixture, rinsed 3 times in methanol and stored at -20°C. For immunofluorescence, embryos were washed three times (10 minutes each) in PBS-T and were then incubated with primary antibodies in the same buffer on a rotating wheel overnight at 4°C. They were washed three times (20 minutes each) in PBS-T. Incubations with secondary antibodies and washing steps were performed identically. Embryos were incubated for 45 minutes in a 2 mg/ml RNAse A solution at 37°C and mounted in Dako fluorescent mounting medium (Agilent, #S3023) containing 2 µg/ml DAPI.

Primary antibodies used were mouse monoclonal anti-V5 (Invitrogen #R960-25, 1:500), mouse monoclonal anti-Flag (clone M2 - Sigma-Aldrich #F3165, 1:1000), rabbit polyclonal anti-acetyl Histone H4 (Merck Millipore #06-589; 1:500), mouse monoclonal anti-histones (Millipore #MABE71; 1:2500), mouse monoclonal anti-PCNA (Abcam #ab29, 1:1000) and rabbit polyclonal anti-GFP (Invitrogen #A-11122, 1:750). Secondary antibodies were used at a 1:1000 dilution and included: Dylight® 488 goat anti-rabbit IgG (Thermo Scientific #35552), Alexa Fluor™ 647 goat anti-rabbit IgG (Invitrogen, # AB-2535813), Alexa Fluor™ 555 goat anti-mouse IgG1 (Invitrogen #AB-2535769), Alexa Fluor™ 488 goat anti-mouse IgG2a (Invitrogen #AB-2535771), Alexa Fluor™ 647 goat anti-mouse IgG2a (Jackson ImmunoResearch #115-605-206). Images were acquired on an LSM 800 confocal microscope equipped with a 40X 1.4 NA objective lens (Carl Zeiss). Images were processed with Zen imaging software (Carl Zeiss), Image J and GIMP.

Generation of a rabbit polyclonal anti-CidB^{wPip} antibody

Two peptides (1158-C+GVSRVYNHSNSRGSR-1172 and 665-C+LRQPRENDLDTHPIG-679; where C+ is a cysteine in the N-terminus position of the peptide added for the coupling to the carrier protein) were designed in conserved regions from an alignment of CidB variants[57]. These peptides were synthesized and injected together into 2 rabbits for immunization (Speedy

28-Day Program, Eurogentec). Specific IgG were affinity purified against the 1158-1172 peptide, and used at a 1:200 dilution for Western-blot and immunofluorescence experiments.

Immunofluorescence and imaging of *Culex* testes

Testes were dissected from 2-day-old males, fixed in PFA 3.2% in PBS-Tween 0.5% for 10 minutes. Tissue permeabilization was increased by adding Heptane (50% v/v) during the fixation step under shaking. After three washes in PBS-Tween, testes were incubated overnight with purified anti-CidB^{wPip} (1:200) and anti-histone MAB3422 (1:200; Sigma-Aldrich) primary antibodies in PBS-Tween 0.5%. Next, testes were washed three times in PBS-Tween and incubated with goat anti-mouse Alexa Fluor^{TM} 488 and goat anti-rabbit Cy3 secondary antibodies (1:500; Invitrogen) for 3 hours at 30°C under agitation. After three washes, testes were mounted with a Vectashield antifade DAPI mounting medium (Vector laboratories), and imaged with a Leica SP5 confocal microscope.

Total protein extraction and western blot on S2R+ cells (for Figure S1)

For each condition, S2R+ cells were plated in a 25 cm^2 culture flask and transfected with 1 µg of plasmid. Cells were harvested one day post transfection and sorted by fluorescence-activated cell sorting (FACS) based on GFP signal above background. 1.10^5 cells were lysed in 100 µl of buffer containing 150 mM NaCl, 10 mM Tris-HCl, 1% sodium deoxycholate, 1% NP40, 0.1% SDS and anti-proteases (Halt; Thermo scientific). Cell lysates centrifuged at 15000g for 30 min at 4°C. Supernatants were collected and protein concentration was estimated by BCA assay (Pierce BCA Assay; Thermo Scientific). 3 µg of total proteins were separated by SDS-PAGE onto 10% polyacrylamide gel and transferred on PVDF membrane (Transblot turbo; Biorad) for Western blot analysis. After saturation in TBS with 0.1% Tween 20 and 5% milk powder, blot was incubated with anti-GFP antibody (1:500; Genscript #A01704-40), followed by a goat anti-rabbit secondary antibody horseradish peroxidase (HRP)-conjugated (1:20000;

Sigma). After revelation, blot was incubated with anti-Tubulin antibody (1:5000) for loading control.

Total protein extraction and western blot on S2R+ cells (for Figure S7)

S2R+ cells were plated in 25 cm^2 culture flask and transfected as above with 1 µg of pAct5C-mkate2-CidA-T2A-sfGFP-CidB plasmid DNA. Cells were harvested at 3-days post transfection and lysed in buffer containing 150 mM NaCl, 10 mM Tris-HCl, 1% sodium deoxycholate, 1% Triton X-100, 0.1% SDS and anti-proteases (Roche). Cell lysates were sonicated briefly and centrifuged at 10 000 g for 10 min at 4°C. Supernatants were collected and stored at -80°C before SDS-PAGE. Protein concentration was estimated by Bradford assay (Coomassie Plus™ Protein Assay Reagent; Thermo Scientific™). Twenty µg of total proteins were separated by SDS-PAGE onto 4–15 % polyacrylamide gel (Bio-Rad) and transferred onto PVDF membranes (Immobilon-P; Millipore) for Western blot analysis. After saturation in PBS with 0.1% Tween 20 and 5% milk powder, blots were incubated with the purified anti-$CidB^{wPip}$ antibody (1:1000; Eurogentec, see above) or anti-GFP antibody (1:10 000; Torrey Pines Biolabs) antibodies, followed by a goat anti-rabbit secondary antibody horseradish peroxidase (HRP)-conjugated (Bio-Rad). Proteins were revealed by chemiluminescence using a ChemiDoc™ Gel Imaging System (Bio-Rad)

Quantification and Statistical Analysis

Flow cytometry analysis was carried out on a mix of non-transfected and transfected cells with each construct. Cells were analysed at day 2 and day 4 post-transfection. We established a growth rate according to the following formula:

$$\text{Log2 (x at Day 4 / x at Day 2)}$$

where x is the proportion of fluorescent cells at the given time-point. A fold change equal or superior to 0 is observed when transfected cells grow at similar rate compared to non-transfected cells. In contrast, a negative fold change reflects a slower growth or cell death

between day 2 and 4. Statistics are based on an ordinary one-way ANOVA test followed by multiple comparisons: mKate2-sfGFP vs. sfGFP:CidB, P=0.0015 n=3; mkate2-sfGFP vs. sfGFP:CidB^{C1025A}, P=0.0057 n=3; mkate2-sfGFP vs. sfGFP:CidB^{C1025R}, P=0.0045 n=3.

Video S1. S2R+ cells expressing sfGFP::CidB and free mkate2. Time is shown in HH:MM. Related to Figure 1.

Video S2. S2R+ cells co-expressing mkate2::CidA and sfGFP::CidB. Time is shown in HH:MM. Related to Figure 1.

Key resources table

REAGENT or RESOURCE	SOURCE	IDENTIFIER
Antibodies		
Rabbit polyclonal anti-CidB^{wPip}	This paper	N/A
Mouse monoclonal anti-V5	Invitrogen -ThermoFisher	Cat#R960-25
Mouse monoclonal anti-Flag (clone M2)	Sigma-Aldrich	Cat#F3165
Mouse monoclonal anti-histone (pan)	Merck Millipore	Cat#MABE71
Rabbit polyclonal anti-acetylated H4	Merck Millipore	Cat#06-589
Mouse monoclonal anti-PCNA [PC10]	Abcam	Cat#ab29
Mouse monoclonal Anti-Histone clone H11-4	Sigma-Aldrich	MAB3422
Rabbit polyclonal anti-GFP	Invitrogen-ThermoFisher	Cat#A-11122
Rabbit anti-GFP	Torrey Pines Biolabs	Cat#TP401
Rabbit polyclonal Anti-GFP	Genscript	A01704-40
TUBA1 monoclonal antibody (M03), clone 2A11	Abnova	H00007277-M03
Goat anti-rabbit HRP-conjugated	Bio-Rad	Cat#170-6515
Alexa Fluor™ 633 Goat anti-Rabbit	Invitrogen -Thermo Fisher	Cat#A-21070
Dylight® 488 goat anti-rabbit IgG (H+L)	Invitrogen -Thermo Fisher	Cat#35552
Alexa Fluor™ 647 goat anti-rabbit IgG (H+L)	Invitrogen -Thermo Fisher	Cat#A-21245
Alexa Fluor™ 555 goat anti-mouse IgG1	Invitrogen -Thermo Fisher	Cat#A-21127
Alexa Fluor™ 488 goat anti-mouse IgG2a	Invitrogen -Thermo Fisher	Cat#A-21131
Alexa Fluor™ 647 goat anti-mouse IgG2a	Jackson ImmunoResearch	Cat#115-605-206
Bacterial and virus strains		
NEB® 5-alpha Competent E. coli	New England Biolab	C2987H
NEB® Turbo Competent E. coli	New England Biolab	C2984H
Chemicals, peptides, and recombinant proteins		
Bovine Serum Albumin	Sigma-Aldrich	Cat#A9647
Q5 polymerase	New England Biolab	M0491S
Q5 site-directed mutagenesis kit	New England Biolab	E0554S
Hoechst 33342	Thermo Scientific™	Cat#62249
Dako mounting medium	Agilent	Cat#S3023
Anti-proteases (cOmplete ™ , Mini, EDTA-free Protease Inhibitor Cocktail)	Roche	Cat#11836170001
4–15% Mini-PROTEAN® TGX™ Precast Protein Gels	Bio-Rad	Cat#4561085
Coomassie Plus™ Protein Assay Reagent	Thermo Scientific™	Cat#23236
Lipofectamine 3000	Invitrogen	L3000008
Critical commercial assays		
Immobilon Crescendo Western HRP substrate	Millipore	#WBLUR0500
NEBuilder Hifi DNA Assembly kit	New England Biolab	E5520S
Deposited data		
Experimental models: Cell lines		

D. melanogaster: Cell line S2R+	Drosophila Genomics Resource Center	FlyBase: FBtc0000150
Experimental models: Organisms/strains		
D. melanogaster. bam-Gal4 (*w ; P{bam-GAL4:VP16}3*)	[42]	N/A
D. melanogaster. topi-Gal4 (*w[*]; M{RFP[3xP3.PB] w[+mC]=topi-GAL4.VP16}ZH-86Fb/TM3, Ser[1]*)	[44], Bloomington Drosophila Stock Center	BDSC: 91776
D. melanogaster. Sgs3-Gal4 (w[1118]; P{w[+mC]=Sgs3-GAL4.PD}TP1)	[41], Bloomington Drosophila Stock Center	BDSC: 6870
D. melanogaster. EG1 (*y w; pUASP-6His-V5-CidA-T2A-Flag-CidB-attP-9A[VK27])/+)*	[29]	N/A
D. melanogaster. DZ41 (*y w; pUASP-6His-V5-CidA-T2A-Flag-CidB[C1025A]-attP-9A[VK27])*	[29]	N/A
D. melanogaster. Wild-Type “Sevelin”	Mia T. Levine	N/A
D. melanogaster. *w; P{w[+mC]=protamineB-eGFP}*	[47]	N/A
D. melanogaster. *w; P{w[+mC]=RPA70-GFP}attP2*	[49]	N/A
Culex quinquefasciatus Slab	Mathieu Sicard	N/A
Culex quinquefasciatus Slab-T	Mathieu Sicard	N/A
Oligonucleotides		
Wolb 16sRNA FOR : 5’TTGTAGCCTGCTATGGTATAACT3’	[56]	N/A
Wolb 16sRNA REV : 5’GAATAGGTATGATTTTCATGT3’	[56]	N/A
Recombinant DNA		
Plasmid: pAc5-fCidA	This paper	N/A
Plasmid: pAc5-fCidB	This paper	N/A
Plasmid: pAc5-fCidA-fCidB	This paper	N/A
Plasmid: pAc5-fCidB_C1025A	This paper	N/A
Plasmid: pAc5-fCidB_C1025R	This paper	N/A
Plasmid: pAc5-mKate2_sfGFP	This paper	N/A
Plasmid: pAc5-RPA3_fCidB	This paper	N/A
Software and algorithms		
ImageJ	Open Source	https://imagej.nih.gov/ij/
ZEN software (blue edition)	Carl Zeiss	https://www.zeiss.fr/
QuickFigures	Open Source	https://github.com/grishkam/QuickFigures
GraphPad Prism 9	GraphPad Software, Inc	RRID:SCR_002798

Zeiss AxioImager Z2/Apotome microscope equipped with suitable filters for the dyes, and a Zeiss ApoTome-slider (63×/1.4 Plan-Apochromat Oil PH3 objective)	Montpellier Ressources Imagerie (MRI) Platform	https://www.mri.cnrs.fr/fr/imagerie-photonique/nos-plateaux/97-mri-dbs/equipements-dbs-optique/microscopie-champ-plein-droit/186-droit-zeiss-z2-apotome.html
ChemiDoc™ Gel Imaging System	Bio-Rad	https://www.bio-rad.com/fr-fr/category/chemidoc-imaging-systems?ID=NINJ0Z15
Zeiss LSM800 confocal microscope (40x1.4 NA objective lens from Carl Zeiss)	Carl Zeiss	https://lymic.univ-lyon1.fr/platim.php

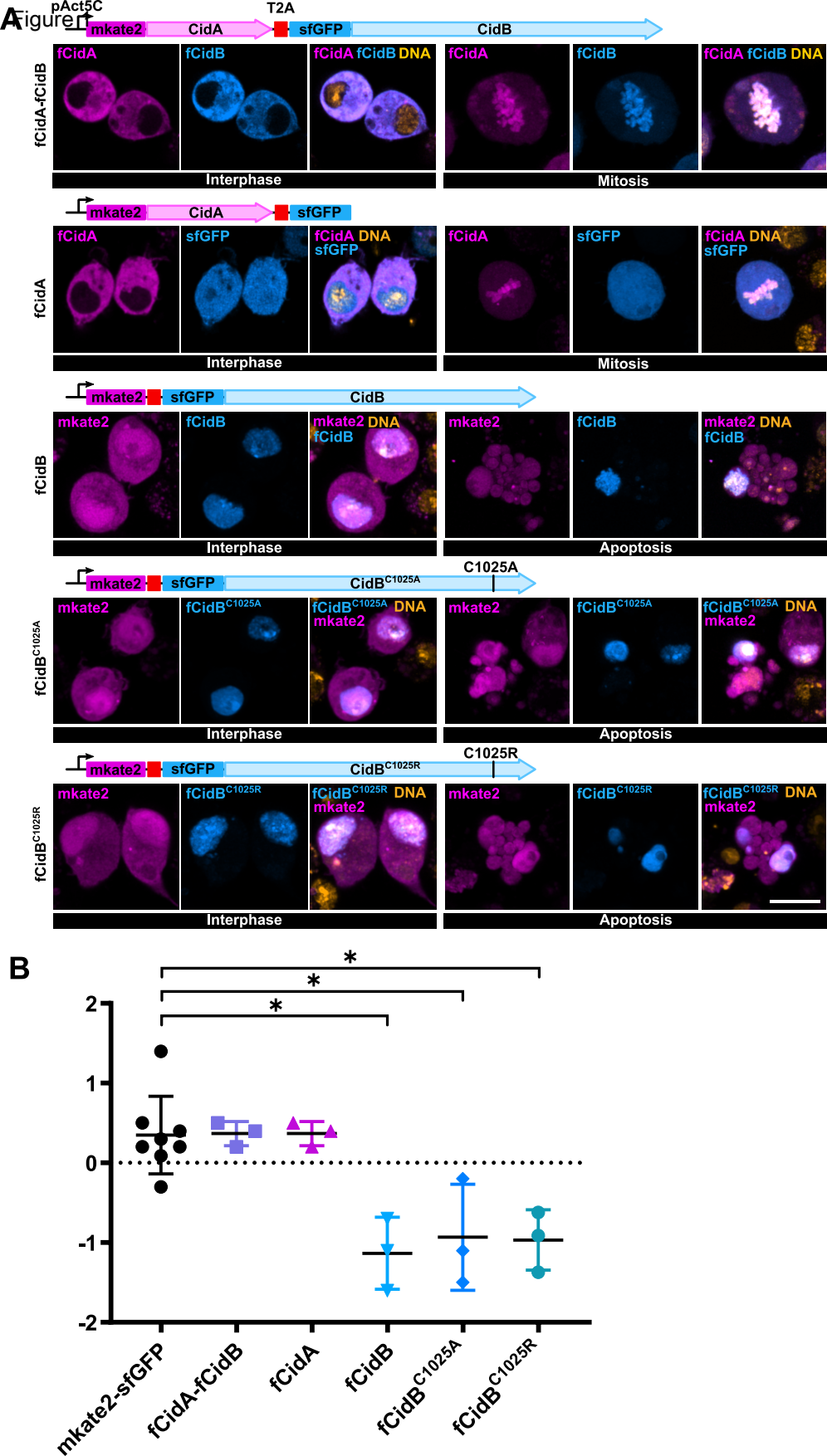
A
Figure
pAct5C
T2A
mkate2
CidA
sfGFP
CidB
fCidA-fCidB
fCidA
fCidB
fCidA fCidB DNA
Interphase
Mitosis
mkate2
CidA
sfGFP
fCidA
fCidA DNA
sfGFP
Interphase
Mitosis
mkate2
sfGFP
CidB
fCidB
mkate2
mkate2 DNA
fCidB
Interphase
Apoptosis
C1025A
CidB^C1025A
fCidB^C1025A
fCidB^C1025A DNA
mkate2
Interphase
Apoptosis
C1025R
CidB^C1025R
fCidB^C1025R
fCidB^C1025R DNA
mkate2
Interphase
Apoptosis
B
*
*
*
2
1
0
-1
-2
mkate2-sfGFP
fCidA-fCidB
fCidA
fCidB
fCidB^C1025A
fCidB^C1025R

Figure 2

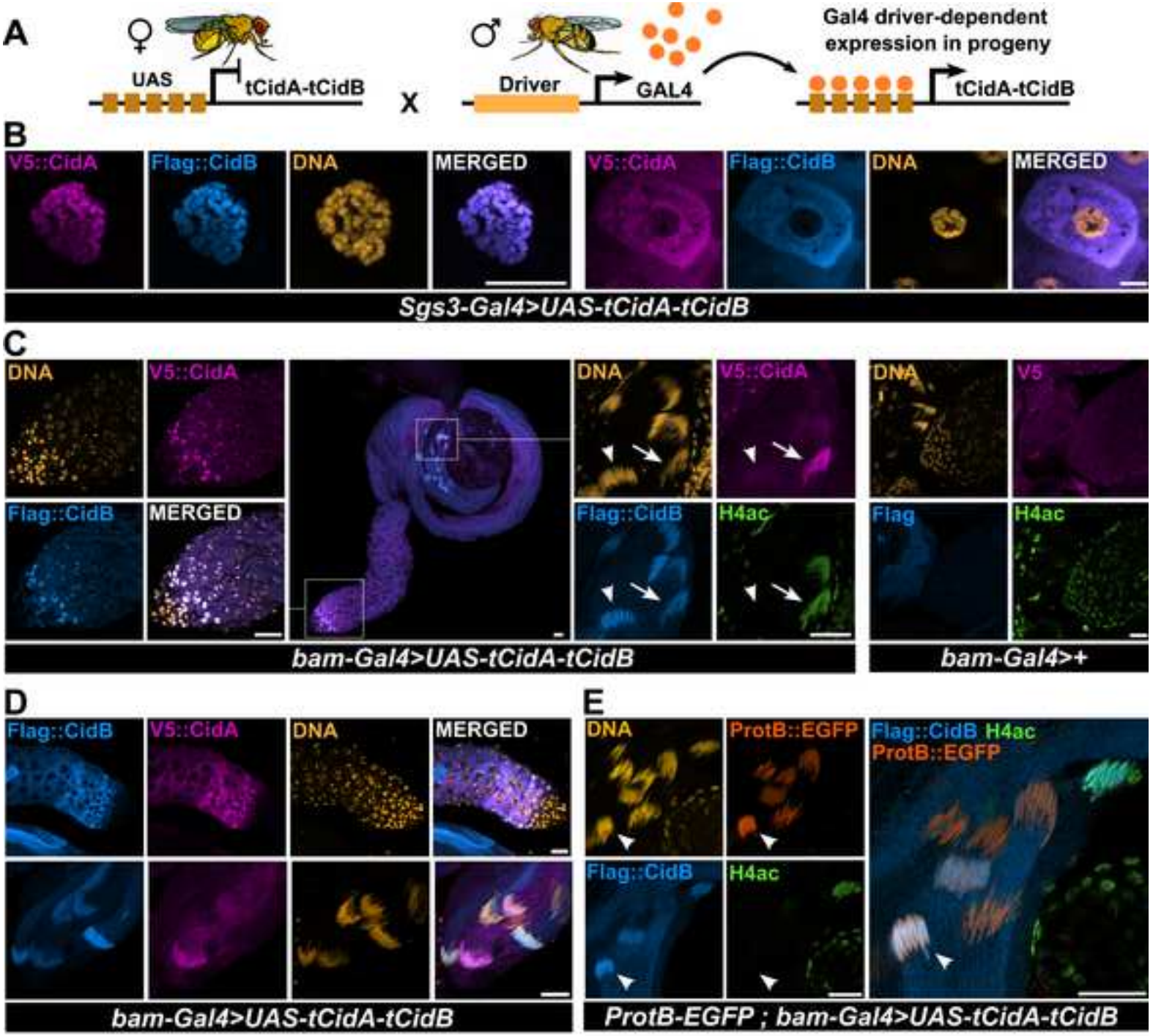

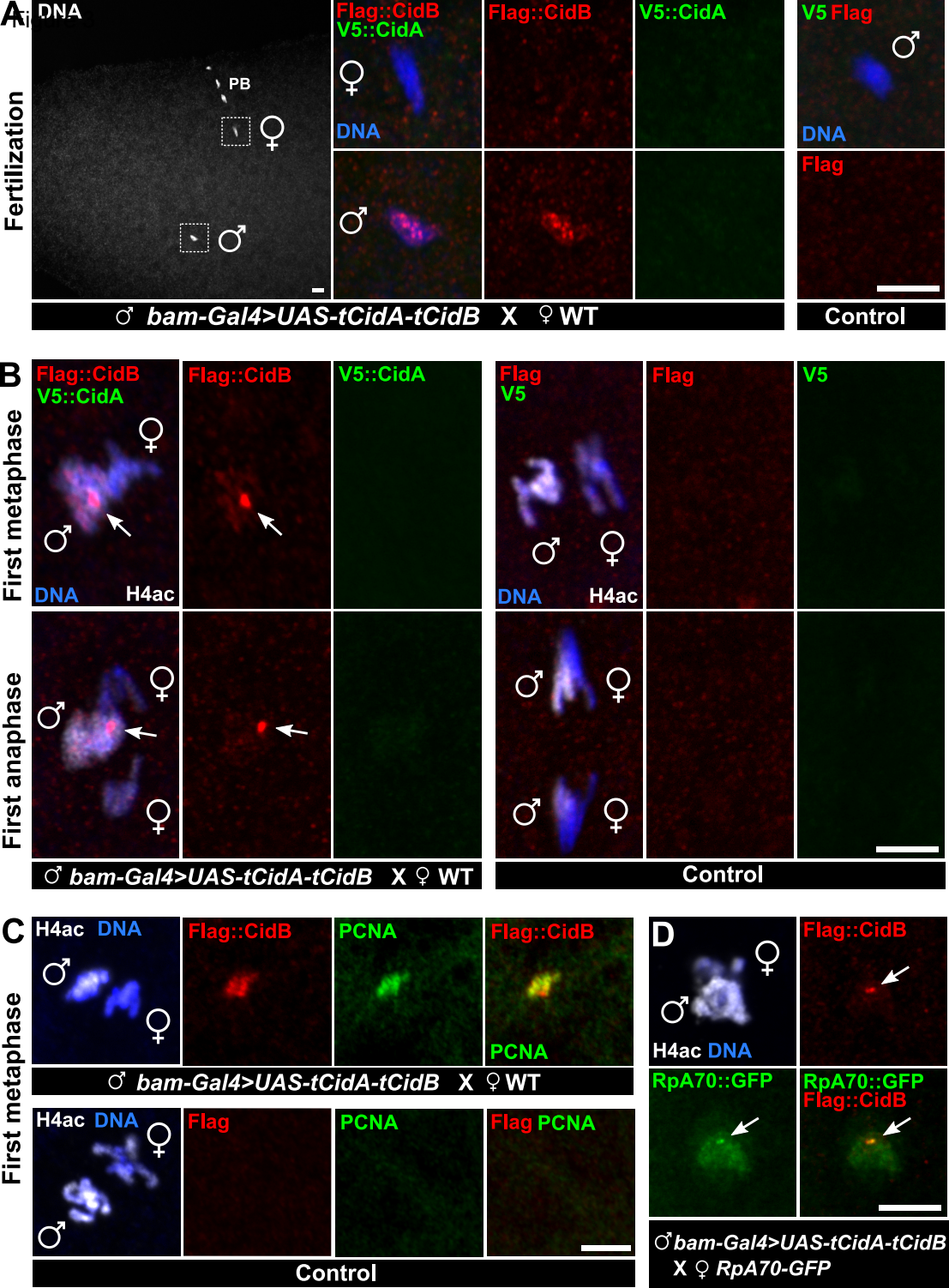
A
Fertilization
DNA
PB
Flag::CidB
V5::CidA
Flag::CidB
V5::CidA
DNA
V5 Flag
DNA
Flag
♂ bam-Gal4>UAS-tCidA-tCidB X ♀ WT
Control
B
First metaphase
First anaphase
Flag::CidB
V5::CidA
Flag::CidB
V5::CidA
DNA
H4ac
Flag
V5
Flag
V5
DNA
H4ac
♂ bam-Gal4>UAS-tCidA-tCidB X ♀ WT
Control
C
First metaphase
H4ac DNA
Flag::CidB
PCNA
Flag::CidB
PCNA
♂ bam-Gal4>UAS-tCidA-tCidB X ♀ WT
H4ac DNA
Flag
PCNA
Flag PCNA
Control
D
H4ac DNA
Flag::CidB
RpA70::GFP
RpA70::GFP
Flag::CidB
♂ bam-Gal4>UAS-tCidA-tCidB
X ♀ RpA70-GFP

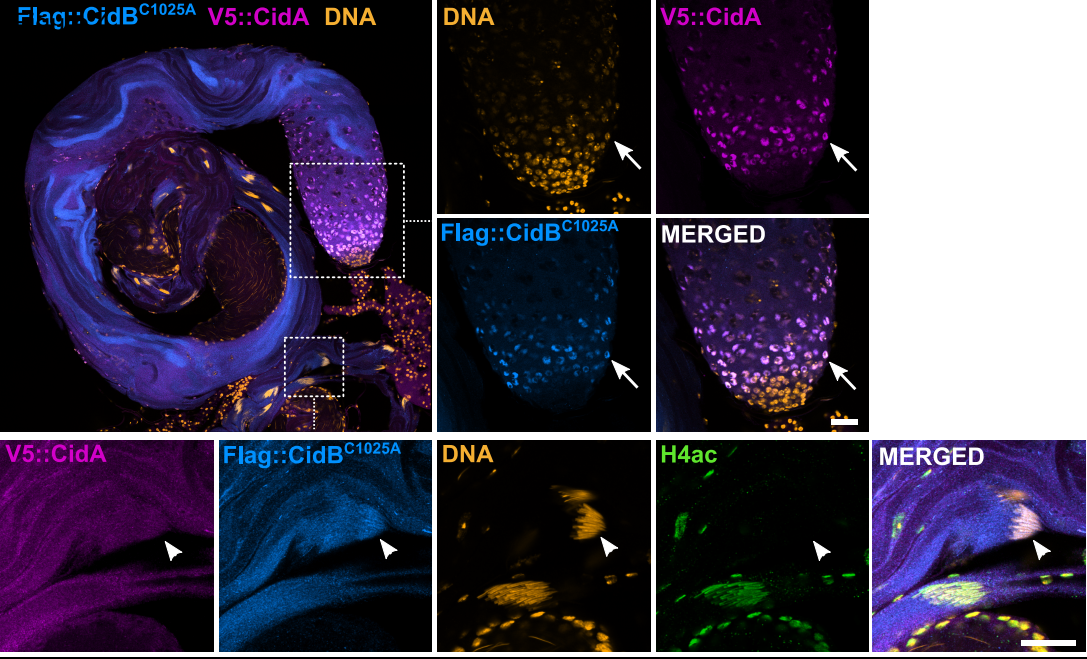

bam-Gal4>UAS-tCidA-tCidB^{C1025A}

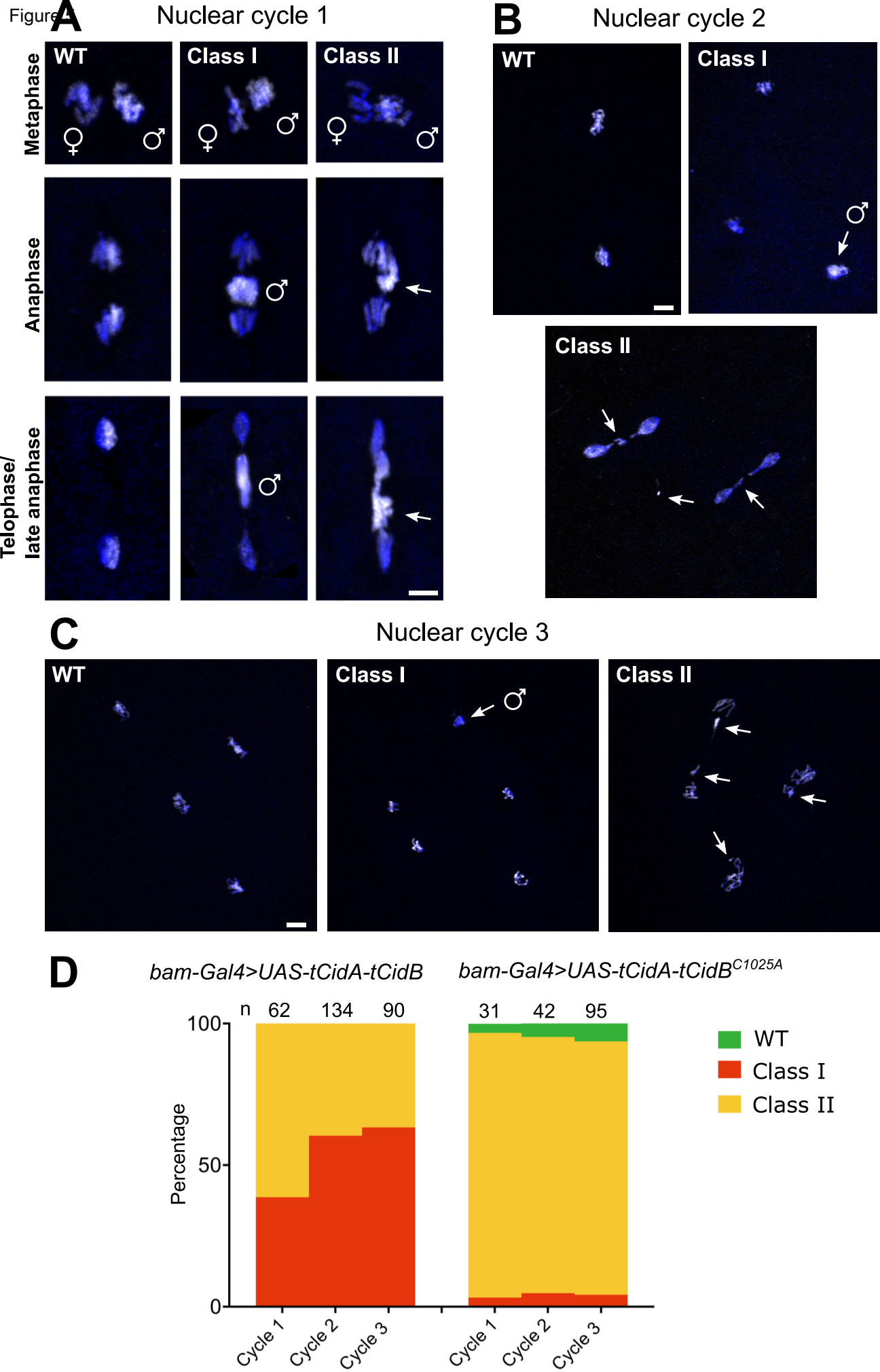
A
Nuclear cycle 1
WT
Class I
Class II
Metaphase
Anaphase
Telophase/
late anaphase
B
Nuclear cycle 2
WT
Class I
Class II
C
Nuclear cycle 3
WT
Class I
Class II
D
bam-Gal4>UAS-tCidA-tCidB
bam-Gal4>UAS-tCidA-tCidB C1025A
n 62 134 90
31 42 95
100
50
0
Percentage
Cycle 1
Cycle 2
Cycle 3
Cycle 1
Cycle 2
Cycle 3
WT
Class I
Class II

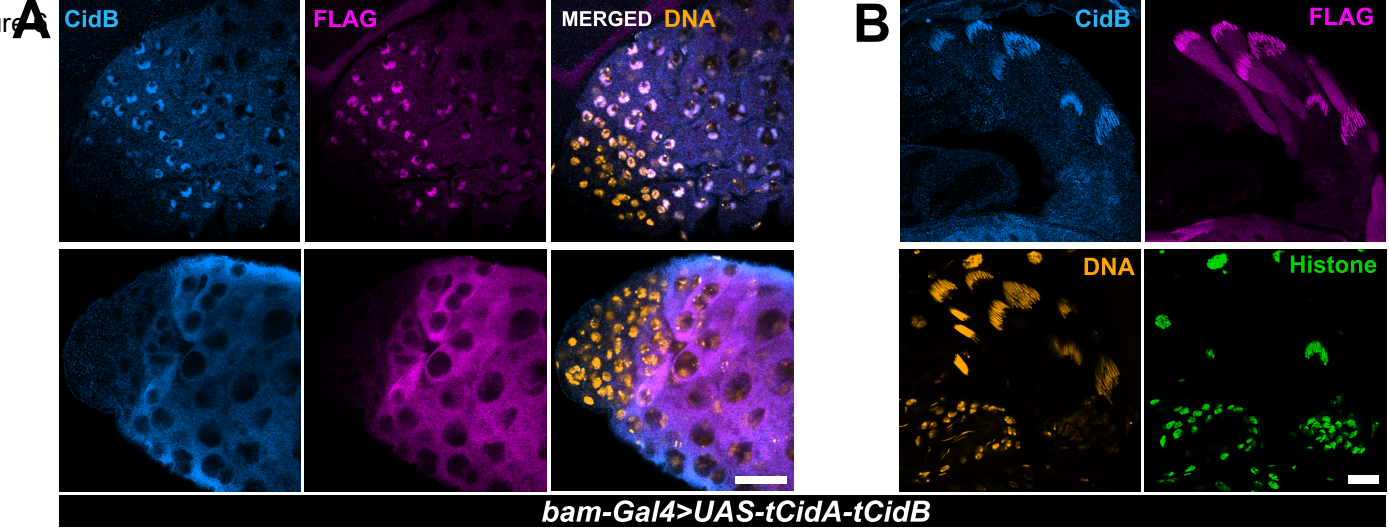
A
CidB
FLAG
MERGED DNA
B
CidB
FLAG
DNA
Histone
bam-Gal4>UAS-tCidA-tCidB

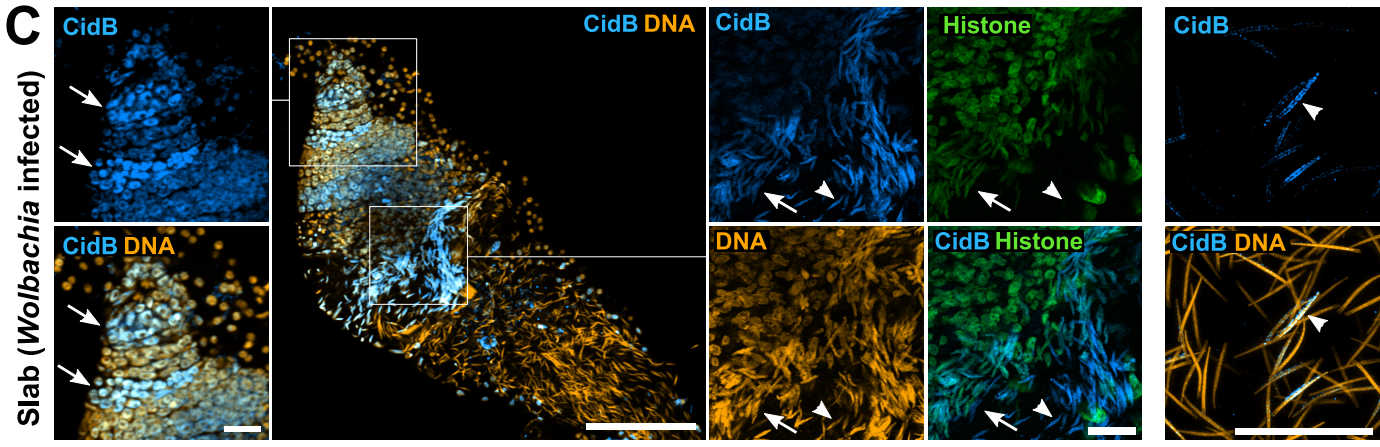
C
Slab (Wolbachia infected)
CidB
CidB DNA
CidB
Histone
CidB
DNA
CidB Histone
CidB DNA

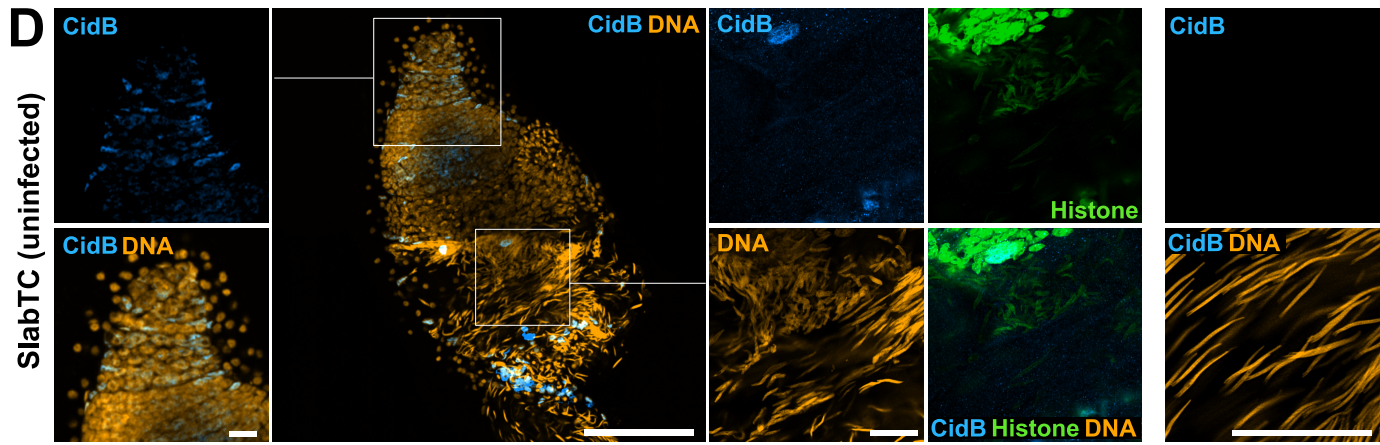
D
SlabTC (uninfected)
CidB
CidB DNA
CidB
Histone
CidB
DNA
CidB Histone DNA
CidB DNA

Table 1 - *Drosophila* embryo hatching rates

Male genotypes	**Female genotypes**	**Number of eggs**	**Hatching rate (%)**
WT	WT	1027	89.5
bam-Gal4>+	WT	1600	89.9
topi-Gal4>+	WT	1042	74.0
+>UAS-tCidA-tCidB	WT	1930	0
bam-Gal4>UAS-tCidA-tCidB	WT	2272	0
topi-Gal4>UAS-tCidA-tCidB	WT	2045	0
+>UAS-tCidA-tCidB$^{[C1025A]}$	WT	1428	88.4
bam-Gal4>UAS-tCidA-tCidB$^{[C1025A]}$	WT	2399	3.4
topi-Gal4>UAS-tCidA-tCidB$^{[C1025A]}$	WT	831	0.1

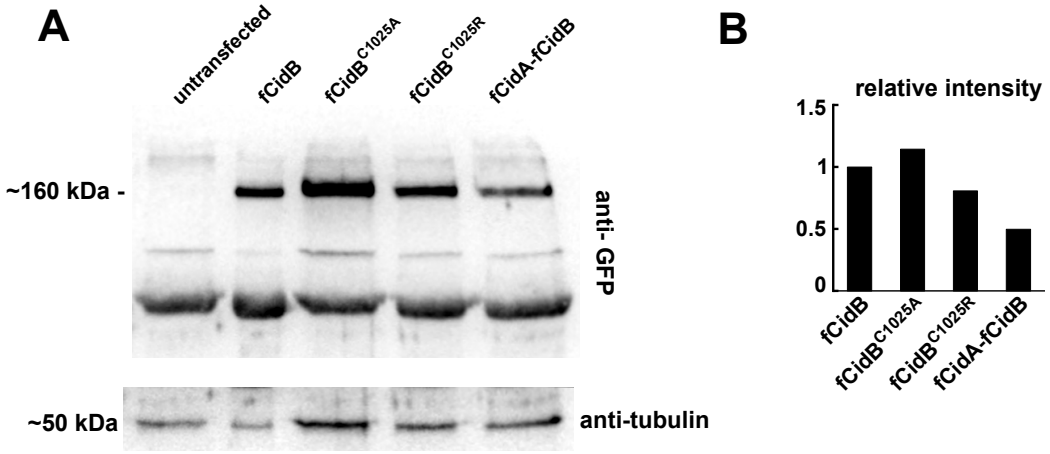

Figure S1 - Western-Blot analysis of fCidB expression in S2R+ cells. **Related to Figure 1.**
(A) Western Blot analysis of protein extracts from S2R+ *Drosophila* cells transfected with the indicated constructs. The sfGFP::CidB fusion protein is detected at the expected size (160.8 kDa) with an anti-GFP antibody. Additional bands are non-specific signals. Anti-α-tubulin is used as a loading control.
(B) Relative signal quantification after normalization with the loading control.

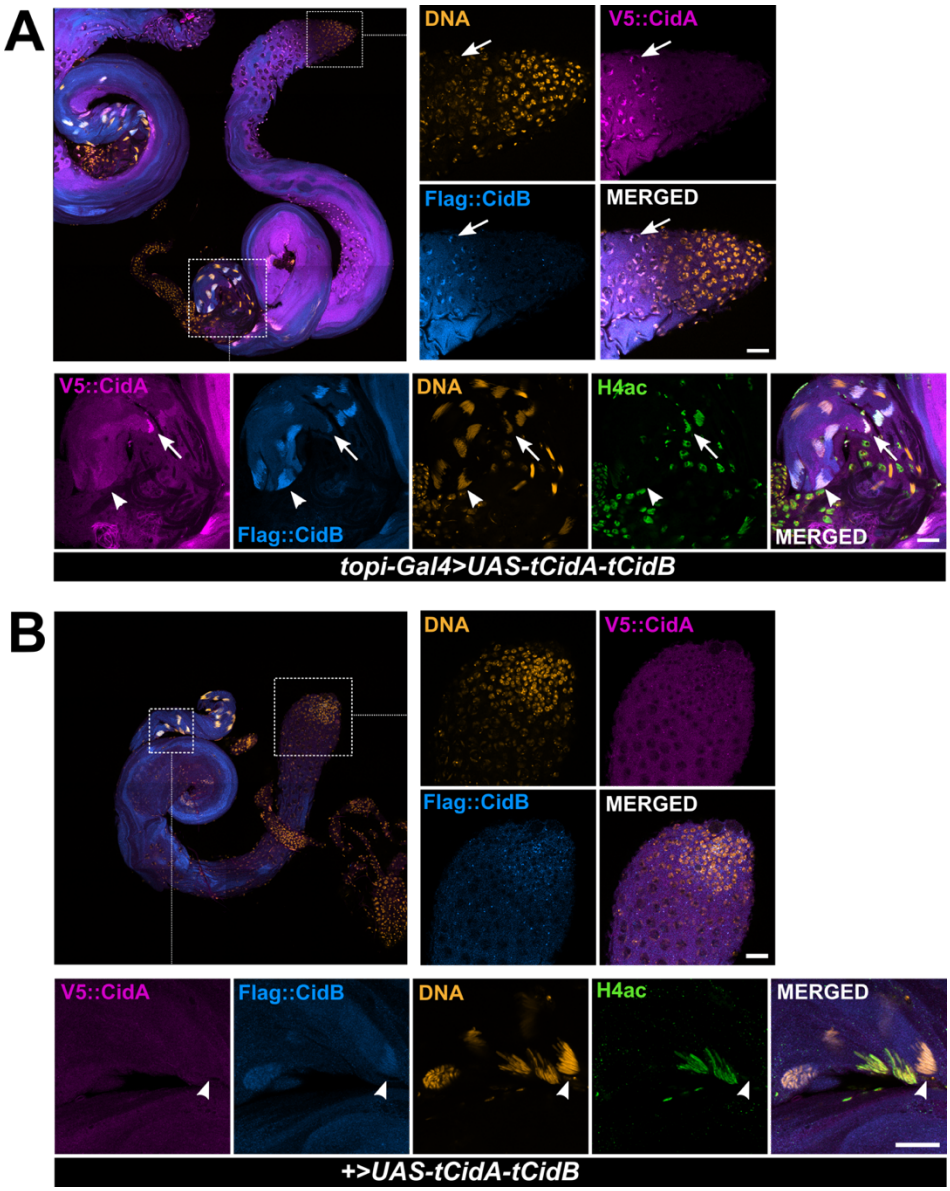

Figure S2 - Distribution of tCid effectors in *topi-Gal4>UAS-tCidA-tCidB* and *+>UAS-tCidA-tCidB* testes. Related to Figure 2.

Confocal images of testes obtained from the indicated cross and stained for Flag::CidB, V5::CidA and acetylated H4 (H4ac).

(A) In *topi-Gal4>UAS-tCidA-tCidB* males, both effectors are first detected in spermatocyte nuclei (arrow in top right panels) but not in earlier germ cells at the apical tip. After meiosis (bottom panels), both V5::CidA and Flag::CidB show the same distribution as in *bam-Gal4>UAS-tCidA-tCidB* males: V5::CidA is most abundant in H4ac positive spermatid nuclei (arrow) but only Flag::CidB is maintained at high levels in post-transition spermatid nuclei (arrowhead).

(B) In *+>UAS-tCidA-tCidB* testes, only background fluorescence is detected in the apical region (top panels). After meiosis (bottom panels), V5::CidA remains undetected and Flag::CidB is only detected at low level in post-transition spermatids (arrowhead). Bars: 20 µm.

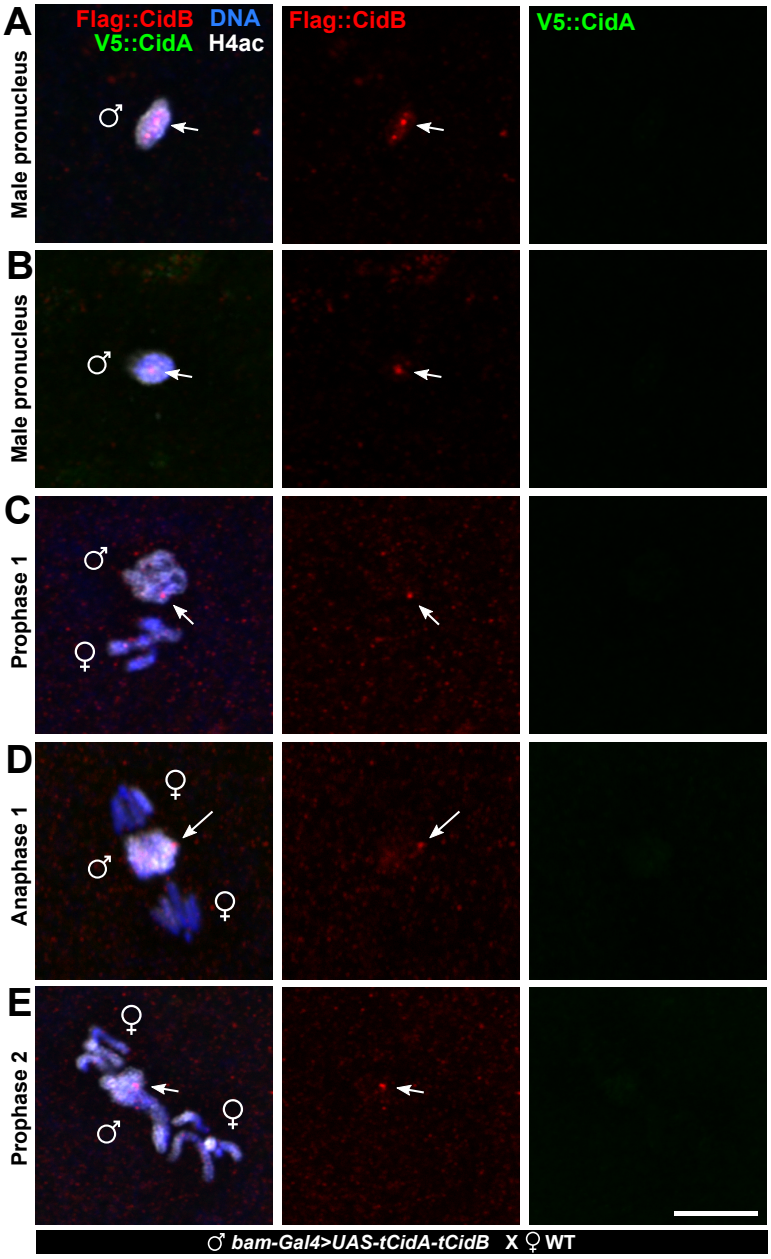

Figure S3 - Additional images illustrating paternal transmission of tCidB. Related to Figure 3.

Confocal images of eggs and embryos from the indicated cross and stained for Flag::CidB, V5::CidA and the paternal chromatin marker histone H4ac.

(A,B) Shortly after fertilization, Flag::CidB is detected as one or several bright nuclear foci (arrow) in the decondensing male pronucleus but V5::CidA remains undetectable.

(C,D) During the first zygotic mitosis, Flag::CidB is typically detected as a unique nuclear focus of variable intensity on paternal chromatin (arrow). Note the paternal chromatin mass that remains on the metaphase plate in anaphase (D).

(E) Flag::CidB can persist on paternal chromatin during the second nuclear cycle. Bar: 10 µm.

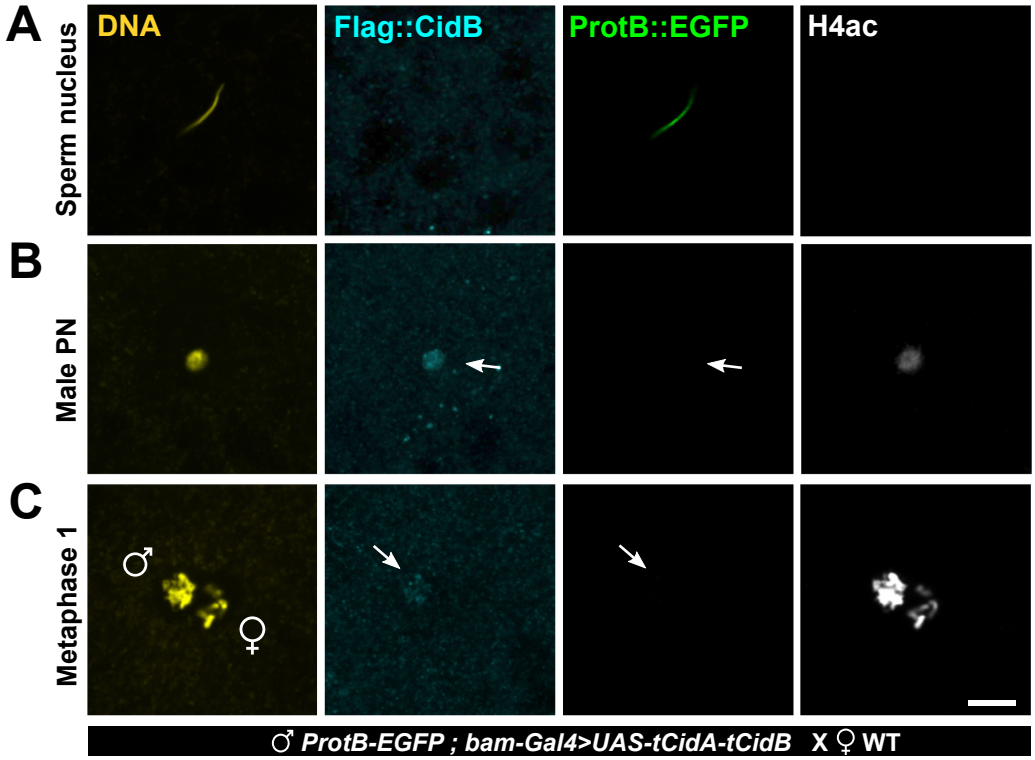

Figure S4 - Protamine removal does not appear affected by paternal CidB. Related to Figure 3.

Confocal images of WT eggs fertilized by sperm from *ProtB-EGFP*; *bam-Gal4>UAS-tCidA-tCidB* males.

(A) A fertilized egg with a non-activated sperm nucleus still packaged with ProtamineB::EGFP. Sperm chromatin is too compact for Flag::CidB immunodetection. Note that defective sperm activation naturally occurs in a small fraction of *Drosophila* eggs.

(B) A round male pronucleus positive for Flag::CidB but negative for ProtamineB::EGFP. Positive H4ac staining indicates that histones have been deposited on the paternal genome.

(C) Flag::CidB persists on paternal chromatin during the first mitosis but ProtamineB::EGFP is not detected. Bar: 10 µm.

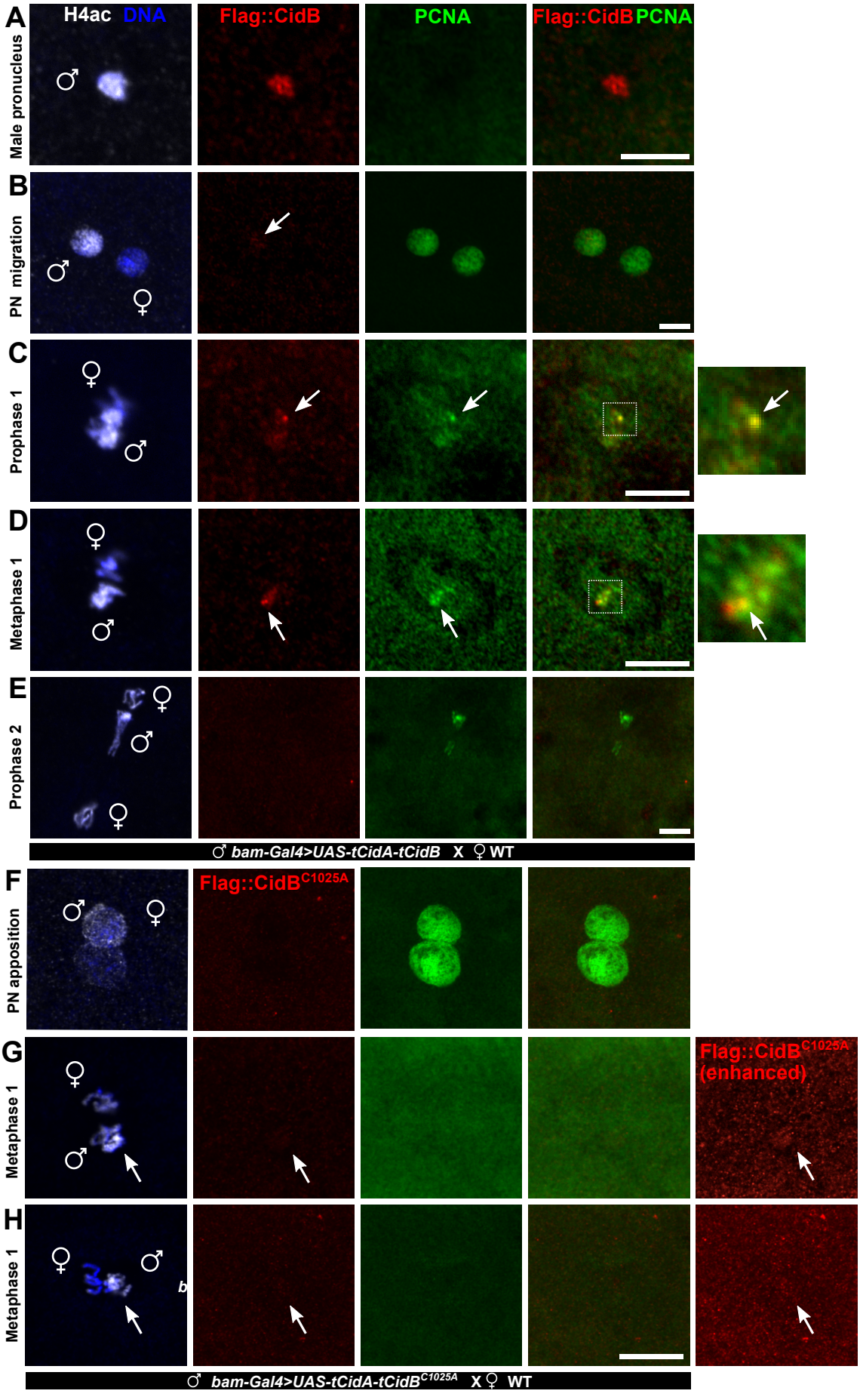
A
Male pronucleus
H4ac DNA
Flag::CidB
PCNA
Flag::CidB PCNA
B
PN migration
C
Prophase 1
D
Metaphase 1
E
Prophase 2
♂ bam-Gal4>UAS-tCidA-tCidB X ♀ WT
F
PN apposition
Flag::CidB C1025A
G
Metaphase 1
Flag::CidB C1025A (enhanced)
H
Metaphase 1
♂ bam-Gal4>UAS-tCidA-tCidB C1025A X ♀ WT

Figure S5 - Distribution of PCNA on paternal chromatin in CI-like *Drosophila* eggs and embryos. Related to Figure 3.

Confocal images of eggs and embryos from the indicated cross and stained for Flag::CidB, PCNA and the paternal chromatin marker Histone H4ac.

(A) Shortly after fertilization and before the onset of the first zygotic S phase, Flag::CidB is always found in the male pronucleus and PCNA is detected in the surrounding egg cytoplasm.

(B) DNA replication begins shortly before pronuclear apposition as revealed by the nuclear accumulation of PCNA in both pronuclei. Note that the Flag::CidB signal (arrow) is typically weak to undetectable on fully decompacted paternal chromatin.

(C,D) During mitosis, PCNA is specifically retained on paternal chromatin and largely colocalizes with Flag::CidB foci (arrows). Yellow color indicates co-localization (insets).

(E) An embryo in prophase of the second nuclear cycle showing the paternal chromatin mass stretched between the haploid maternal nuclei. Flag::CidB is no longer detected in this case but PCNA persists on paternal chromatin.

(F) Pronuclear apposition in an egg fertilized by sperm from a *bam-Gal4>tCidA-tCidB*^{C1025A} male.

(G) Using the same settings as in (A-E), Flag::CidB^{C1025A} and PCNA are not detected above background on paternal chromatin during the first mitosis. However, enhancing the red signal potentially reveals low level of Flag::CidB^{C1025A} on paternal chromatin (arrow, right panel).

(H) Another embryo at the same stage with the same staining and enhancing.

Paternal chromatin is identified with the H4ac marker. Bar: 10 μm.

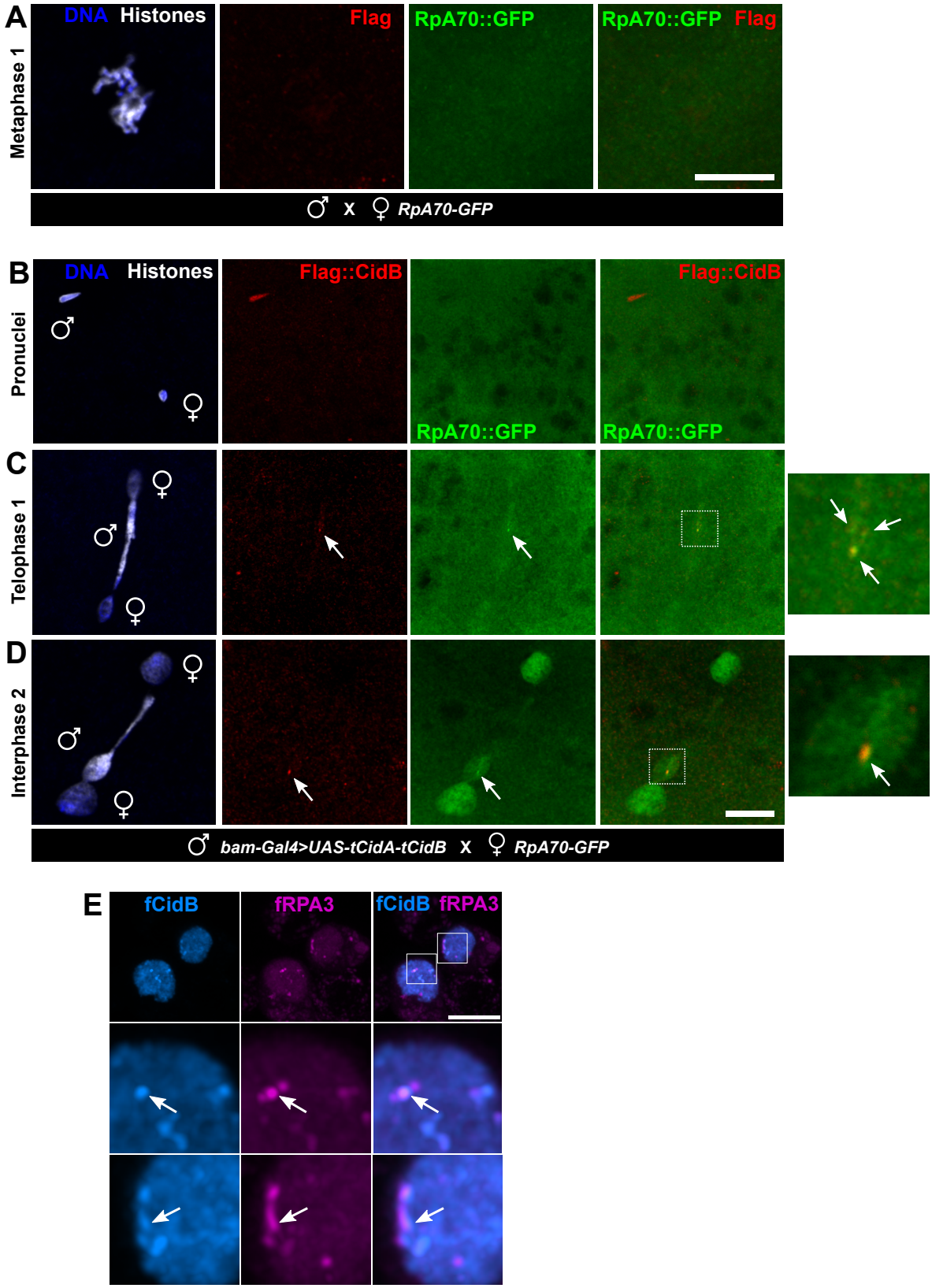

Figure S6 – CidB associates with the replication stress marker RpA. Related to Figure 3.
(A) In control embryos from the *RpA70-GFP* stock, RpA70::GFP is never detected on chromosomes during the first mitosis (0%, n=8).

(B) In *RpA70-GFP* eggs fertilized by sperm from *bam-Gal4>UAS-tCidA-tCidB* males, RpA70::GFP is not detected in the pronuclei. Note the presence of Flag::CidB (red) in the decondensing male pronucleus.
(C) In telophase of the first mitosis, several Flag::CidB foci are detected in the paternal chromatin bridge (arrows) and each one is associated with RpA70::GFP (green).
(D) During the second S phase (interphase), RpA70::GFP accumulates in both daughter nuclei of maternal origin, but is also enriched on the Flag::CidB focus on paternal chromatin (arrow). Yellow color indicates co-localization (insets). Bar: 10 μm.
(E) Confocal image of representative S2R+ cells transfected with *pAct5C-mkate2-RPA3-T2A-sfGFP-CidB*. Arrows in insets indicate colocalization of mKate2::RPA3 with fCidB. Bar: 10 μm.

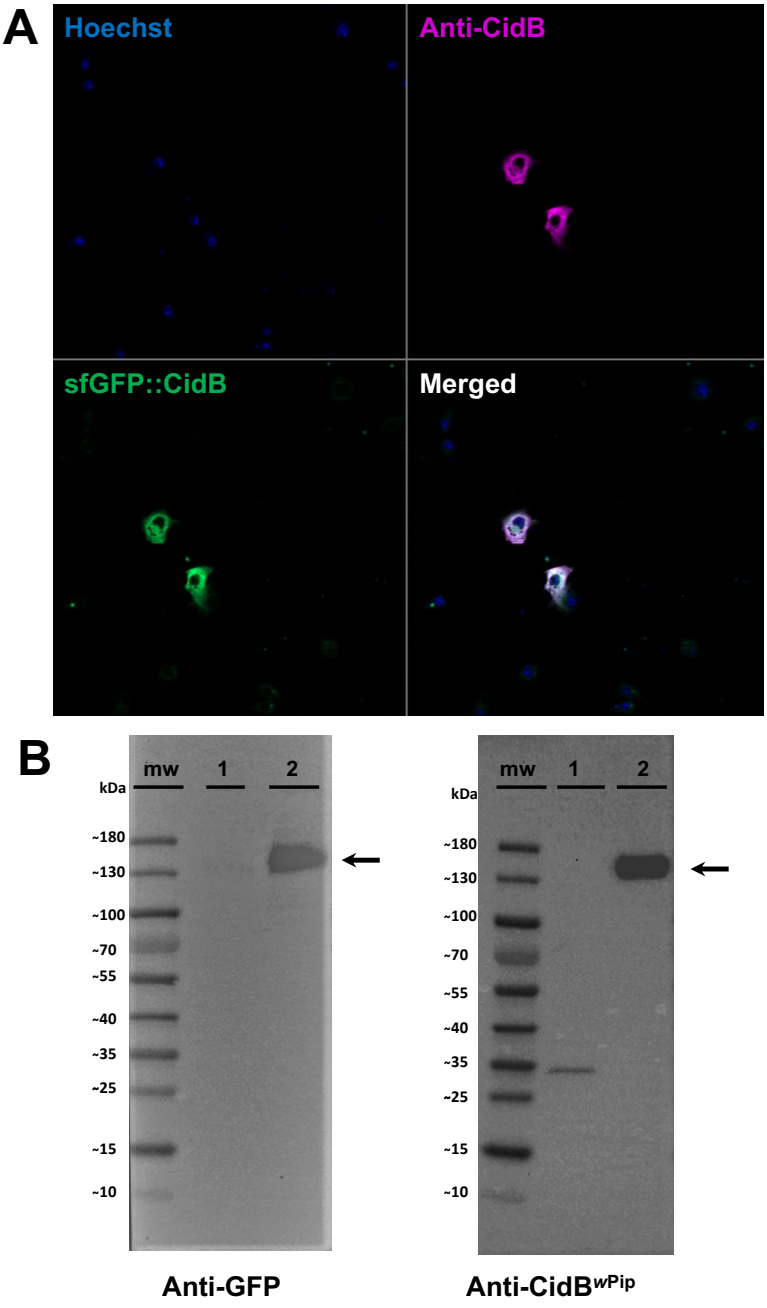

Figure S7 - Characterization of a rabbit polyclonal anti-CidB^{wPip} antibody. Related to Figure 6.

(A) Confocal image of S2R+ *Drosophila* cells transfected with pAct5C-*mKate2-CidA-T2A-sfGFP-CidB* and stained with the purified anti-CidB^{wPip} antibody. Only transfected cells show an anti-CidB signal, which colocalizes with native sfGFP::CidB fluorescence.

(B) Western-Blot analysis of indicated protein extracts from S2R+ *Drosophila* cells. The sfGFP::CidB fusion protein (expected size 160.8 kDa) is detected by both anti-GFP (left) and anti-CidB (right) antibodies.